Candida albicans as a Biochemical Computer:

Cross-Kingdom Signaling, Parasexual Reproduction, and Genetic Foundations of a Unique Fungal Symbiont

Jim Craddock
Redacted Science Research Initiative
redactedscience.org | jimcraddock.com
May 2026
V13

Abstract

Candida albicans functions as a distributed biochemical computer, processing host and environmental signals through multiple parallel channels to modulate immunity, metabolism, tissue remodeling, and endocannabinoid tone. This paper details its distinctive genetic hardware (~1,300 orphan genes with no orthologs in other yeasts), ancient CUG codon reassignment (~171 ± 27 Ma), divergence from *C. dubliniensis* with asymmetric gene-family expansion (~20 Ma), parasexual cycle for rapid diversity generation, and layered signaling architecture (extracellular vesicles with morphology-dependent cargo, candidalysin and Ece1 peptide panel, secreted aspartyl proteases, cholinergic receptor interface, authentic prostaglandin E_2 production from host arachidonic acid, cross-kingdom RNA potential, tryptophan-kynurenine pathway modulation, mast cell activation via cell wall pattern recognition, direct modulation of host metabolic state through suppression of plasma leptin (Peroumal *et al.*, 2022), elevation of apolipoprotein-B-containing lipoproteins via formyl-methionine–HIF-2α–ceramide signaling (Wang *et al.*, 2024), a dopaminergic signaling intersection through the Gpr1 receptor), bile acid signaling through organism-driven depletion of bacterial deconjugators with downstream FXR-mediated suppression of host antifungal defenses (Thangamani *et al.*, 2021), capture of host complement regulators C4BP, factor H, and FHL-1 on the fungal surface to evade complement-mediated killing across all three pathways (Meri *et al.*, 2004)). The host serum proteome carries selected counter-measures: apolipoprotein-B contains embedded antifungal cryptides that damage the fungal surface (Dell-Olmo *et al.*, 2021), and hepcidin combines iron sequestration with direct antimicrobial peptide activity against *C. albicans* (Arekar *et al.*, 2025; Chen and Lan, 2020). Both are bypassed in hosts with compromised liver function or low circulating apoB-cryptide load.

The hybrid origin of *C. albicans* from a Miocene fusion of two parental lineages at approximately 2.8% sequence divergence (Mixão and Gabaldón, 2020) is integrated here as the source of the chimeric genome architecture: loss of heterozygosity fixes host-calibrated input sensors to a single optimized version while retained ancestral heterozygosity at effector, adhesion, efflux, and phenotypic-switch loci supports combinatorial output — a committed-input, parallel-output design consistent with distributed biochemical computation. Multi-input convergence nodes execute the integration: the adenylyl cyclase Cyr1 sums CO_2, bacterial peptidoglycan, and farnesol of opposite valence into cAMP-PKA morphogenetic decisions (Hall *et al.*, 2010; Xu *et al.*, 2008; Davis-Hanna *et al.*, 2008); the Ras-like GTPase Rsr1 integrates galvanotropic, thigmotropic, and mechanical cues into calcium-dependent polarity decisions (Brand *et al.*, 2008, 2007). Two parallel second-messenger architectures operate simultaneously in the same cell. The organism's extracellular vesicle output channel, now documented to reach the central nervous system via the nasal-mucosal route in mammalian therapeutic contexts (Madhu *et al.*, 2026), is proposed as a chronic endogenous delivery vector of the colonized state, with inverse valence relative to the therapeutic reference.

The interstitium, a body-wide network of fluid-filled collagen-lined compartments (Benias *et al.*, 2018), is identified as the physical distribution layer connecting peripheral colonies to host nutrient interfaces and enabling inter-niche signal propagation without bloodstream exposure. Hyphal transit through this distribution layer produces mechanoreceptor activation detectable as formication, currently misclassified as psychiatric and responsive to bedside mechanical and pharmacological tests inconsistent with central perceptual origin. Multi-timescale epigenetic memory, from white-opaque phenotypic locking to chromatin-level bet-

hedging and mitochondrial genome methylation, enables state maintenance without genomic change. Beneath the memory layers, a chromatin state-machine substrate executes transitions between operational modes: a multi-acyl-CoA post-translational modification panel covering 17.5% of the proteome (Zhou *et al.*, 2021) integrates metabolic-state inputs through shared writer/reader/eraser hardware, while CTG-clade-specific chromatin innovations — the variant histone H3V^CTG^ and specialized RSC remodeler subunits — operate on the same substrate to balance commensal and pathogenic states (Rai *et al.*, 2019; Brahma *et al.*, 2023; Joshi *et al.*, 2026). Single chromatin enzyme deletions abolish virulence (Shivarathri *et al.*, 2019), establishing chromatin as the substrate the integrated program runs on.

The pituitary microadenoma, conventionally classified as a benign incidental neoplasm with a prevalence of 14-22% in autopsy and radiological studies, is reinterpreted here as a tissue stress response to sustained organism-driven governance load on the anterior pituitary, supported by documented hyphal access to the gland, confirmed molecular machinery for local hormone transport, sequestration, and enzymatic modification, an epidemiological profile consistent with variable organism demand rather than spontaneous neoplasia, and a longitudinal case study documenting microgranuloma formation, hyphal migration to the pituitary region, and subsequent structural failure under escalating load across four transition phases (Craddock, Hemodynamic Decompensation). Pharmacovigilance data further confirm the governance architecture: azole antifungals produce endocrine cascades whose breadth and specificity track the drug's inhibitory profile against organism-host enzymatic nodes (11β-HSD2, 11β-hydroxylase, CYP17A1), with reporting odds ratios exceeding 800 for posaconazole-associated apparent mineralocorticoid excess and a clean mechanistic split between azoles that hit these nodes and those that do not. Standard diagnostic panels compound this invisibility: urine bicarbonate, the most informative marker for the renal tubular acidosis this governance predicts, was removed from routine urinalysis, and creatinine-based renal filtration estimates systematically overestimate function in any subject whose muscle mass is declining under organism-driven substrate progression

No other organism is known to combine this full toolkit. Sixteen testable predictions, grouped by architectural layer, are offered to evaluate the model, including hybrid-origin bimodal orphan ancestry test, host-mediated subroutine termination via glucose override, and chronic apoB-suppression therapy producing measurable mycobiome shifts in patients with concurrent hepcidin axis compromise. The conventional "opportunistic pathogen" classification is re-examined; the organism appears tuned for regulated, long-term persistence rather than unchecked exploitation. This technical grounding is straightforward and stands on its own.

Keywords: Candida albicans; biochemical computer; cross-kingdom signaling; orphan genes; CUG codon reassignment; parasexual cycle; bet-hedging, extracellular vesicles; candidalysin; Ece1 peptides; cholinergic interface; prostaglandin E_2; arachidonic acid competition; Hgt4 glucose sensor; peptide transporters; spatial multiplexing; host adaptation; phenotypic switching memory; tryptophan-kynurenine modulation; mast cell degranulation; Gpr1 dopaminergic interface; mitochondrial epigenetics; symbiont; volatile organic compounds; interstitium; extracellular space; connective tissue; fibroblasts; receptors; purinergic; fatty-acids; medium-chain; antifungal agents; basement membrane; dermis; keratinocytes; pituitary microadenoma; hypophyseal governance load; local hormone multiplexing; hybrid origin; loss of heterozygosity; ancestral heterozygosity; committed-input parallel-output architecture; EV-mediated CNS Modulation, diagnostic gap; chromatin state-machine; writer/reader/eraser

hardware; multi-acyl-CoA modification; lysine crotonylation; H3V^CTG^ variant histone; CTG-clade chromatin innovation; RSC remodeling complex; biofilm chromatin lockdown; cAMP-PKA convergence node; Cyr1 multi-input integration; bacterial peptidoglycan sensing; farnesol mixed-valence input; galvanotropism; thigmotropism; Rsr1 polarity landmark; calcium-dependent integration; parallel second-messenger architecture; hepcidin antimicrobial peptide; iron homeostasis; apoB cryptides; host counter-measure architecture; complement evasion; C4BP capture; factor H binding; Pra1; Hgt1p; bile acid signaling; FXR; ASBT; taurocholic acid; mycobiome stratification; apoB suppression prediction; formication; subcutaneous hyphal transit; mechnoreceptor activation; dermatozoenwahn category error; Ekbom syndrome reframe; topical antifungal kinetics; psychiatric misclassification; bidirectional electrolyte governance; antifungal-induced endocrine cascade; intrasellar fungal abscess; pituitary pattern recognition receptors; somatomammotroph glucan response; prolactin fungal induction; amino acid alkalinization; Stp2 SPS sensor system; white-opaque ancestral program; carbon-source state input; arachidonic acid branch point confirmation

1. Introduction

A biochemical computer is defined here as a biological system that (1) senses environmental and host-derived inputs, (2) integrates multiple signals via internal regulatory states, (3) produces adaptive outputs, and (4) maintains state across time through memory mechanisms such as epigenetic or phenotypic locking. These properties satisfy standard criteria for information-processing systems as defined in biological signaling literature.

Candida albicans meets these criteria. Conventionally labeled an "opportunistic pathogen," the fungus is in fact an obligate commensal with no known environmental reservoir outside mammalian hosts. It colonizes the gastrointestinal tract of a large percentage of healthy individuals and possesses an extraordinary suite of capabilities that extend far beyond simple opportunism.

This paper argues that the "opportunistic pathogen" label understates the organism's true nature. Rather than a passive opportunist, *C. albicans* operates as a distributed biochemical computer: it continuously senses host conditions through dedicated input channels, integrates signals via parallel metabolic and regulatory pathways, produces context-specific adaptive outputs, and maintains heritable phenotypic states. The goal is to present the genetic foundations, reproductive strategy, and signaling architecture in a standalone, technically rigorous manner. Among the framework reinterpretations developed in this paper, the pituitary microadenoma — currently classified as a benign incidental neoplasm in 14–22% of the population (Section 4.7) — is reframed as a tissue stress response to sustained organism-driven governance load, with epidemiological, mechanistic, and longitudinal-case-study support.

2. Genetic Foundations & Evolutionary Origins

The genetic architecture of *C. albicans* supplies the foundational hardware. One of the most distinctive features is the CUG codon reassignment (~171 ± 27 Ma; Mühlhausen *et al.*, 2016) in the ancestor of the CTG clade. The CUG codon switched from leucine to serine via an ambiguous intermediate tRNA (Santos *et al.*, 1995). Strong AT bias fixed the new system, while residual low-level mistranslation (~3% leucine incorporation at CUG sites; Bezerra *et al.*, 2021)

introduced proteomic diversity useful for early bet-hedging under stress. This reassignment enabled expansion of novel protein families central to host interaction.

Approximately 20 million years ago, in the early Miocene, *C. albicans* diverged from *C. dubliniensis*. *C. albicans* expanded gene families associated with host interaction and virulence, while *C. dubliniensis* followed a reductive path. Roughly 1,300 genes (~21% of the ~6,200 protein-coding genes) have no clear orthologs in other yeasts (Butler *et al.*, 2009); many are predicted to support GPCR ligands, immune modulation, and neuropeptide-like sequences.

Recent population-scale genomic analysis has revealed that *C. albicans* is not merely a highly heterozygous diploid but a descendant of a single hybridization event between two divergent parental lineages (Mixão and Gabaldón, 2020). Comparison of heterozygous blocks across *C. albicans* isolates from deeply divergent clades established that approximately 80% of the specific allelic differences are shared across clades — that is, ancestral rather than accumulated post-divergence. The magnitude of divergence between homeologous chromosomes in the inferred heterozygous ancestor is estimated at 2.8%, a level incompatible with vertical evolution from a single lineage under standard mutation rates and inconsistent with continuous gene flux from lineage-specific admixture events. The pattern is what would be expected if two diverged parental lineages fused into a single hybrid ancestor that then gave rise to all extant *C. albicans* isolates.

The hybrid origin is further supported by the demonstration that C. africana and C. stellatoidea share the same hybrid ancestor with *C. albicans* (Mixão *et al.*, 2021), now descending as three parallel lineages from the original fusion event. *C. dubliniensis*, the closest sister species, shows no hybrid signature and followed a reductive evolutionary trajectory with extensive gene loss. Because *C. dubliniensis* is not a hybrid, the hybridization event must have occurred in the *C. albicans* lineage after its split from *C. dubliniensis* (20 Ma as described above) and before the radiation of the hybrid descendants. This brackets the hybridization to the Neogene, most plausibly the Miocene — a window that coincides approximately with the emergence of the great ape lineage (18–15 Ma), though any causal relationship between the two events remains to be tested. "The cross-mammalian extension of this evolutionary architecture is developed separately (Craddock, Pan-Mammalian), and the framework now recognizes the conserved feature across the mammalian clade as the interface architecture itself rather than the identity of any single organism. Each mammalian lineage carries its own host-adapted Saccharomycetaceae symbiont — C. albicans in humans, C. natalensis in dogs, C. tropicalis in mice, Kazachstania slooffiae in pigs — with the partnership architecture documented in this paper representing the human instance of a pattern conserved across the mammalian body plan. The findings developed here at the C. albicans level should be read as one well-characterized instance of a clade-wide partnership architecture rather than as C. albicans-specific phenomena."

2.1 Functional Consequences of Fused Lineage Hybridization

The functional consequence is substantial. Shortly after hybridization, the ancestral lineage lost the capacity for efficient sexual reproduction, locking the organism into clonal and parasexual propagation. This is not an incidental feature. Clonal reproduction preserves the chimeric heterozygosity of the hybrid ancestor by preventing recombination that would collapse allelic variation. Every modern *C. albicans* cell inherits the ancestral two-parental-lineage architecture. Loss of heterozygosity (LOH), discussed in Section 2.2, is the mechanism by which cells can commit to one or the other parental allele at specific loci. Parasexuality (Section 3) is

the mechanism by which variation is generated under stress without compromising the baseline hybrid substrate. The hybrid origin and the reproductive strategy are the same event viewed from two angles.

The approximately 1,300 *C. albicans*-specific orphan genes referenced above should be reconsidered in this light. Under the hybrid-origin model, these genes are not unique innovations of a single lineage; they are the combined contributions of two parental lineages, assembled into a chimeric genome at the time of fusion. This is directly testable with genomic foundation models and is added as Prediction 2b in Section 5.1

2.2 The Committed-Input / Parallel-Output Architecture

The hybrid-origin model predicts that modern *C. albicans* should carry a patchwork genome: heterozygous blocks where the two ancestral haplotypes are retained in parallel, alternating with LOH regions where one haplotype has been fixed and the other lost (Muzzey *et al.*, 2013; Hirakawa *et al.*, 2015; Ropars *et al.*, 2018). This raises a functional question. Which genes are retained heterozygous, and which are committed to a single allele? If the distribution were random, it would carry no framework-level information. If the distribution is functionally structured, it reveals how the hybrid substrate has been organized as a computational architecture.

Published locus-level characterization of major signaling and host-interaction genes reveals a consistent pattern.

The Hgt4 glucose sensor (ORF19.5962, chromosome 5) sits in an LOH region. The two "alleles" of HGT4 are identical across the 2.247-kb coding region plus 1 kb of upstream and downstream flanking sequence (Brown *et al.*, 2006). A single committed version of the glucose sensor, calibrated to approximately 5 mM extracellular glucose, is present in every cell. This is the expected configuration for a reference-calibration component: if the glucose sensor is to accurately report extracellular glucose relative to the human serum set point, the two alleles cannot be allowed to drift to slightly different calibrations. One optimized version, fixed by LOH early in the lineage history, preserves the precision of the input.

This architectural commitment extends beyond Hgt4 alone. The Hgt protein family deploys a multifunction pattern at the cell surface: Hgt1, the family member characterized as a high-affinity glucose transporter, doubles as a complement evasion molecule binding both Factor H and C4b-binding protein, comprehensively interfering with all three complement activation pathways (Lesiak-Markowicz et al., 2011; Harpf et al., 2020). The same gene family supplies the LOH-fixed glucose reference sensor and the host-side partnership-management protein. Selection has tuned one family for two structurally important jobs — environmental input sensing in Hgt4, partnership management in Hgt1 — rather than evolving separate gene families for each function. The §4.3 treatment of complement evasion develops the Hgt1 finding in its host-interaction context.

The output and effector genes show the opposite pattern. The secreted aspartyl proteases SAP1 and SAP2 (chromosome R), and SAP4, SAP5, SAP6 (chromosome 6) are heterozygous, with alleles distinguishable by restriction polymorphism (Staib *et al.*, 2000; Staib and Morschhäuser, 2010). SAP2 alleles are functionally divergent in their regulatory response: basal expression of the SAP2-2 allele, but not SAP2-1, provides the proteolytic degradation products that serve as inducers for full SAP2 induction (Staib and Morschhäuser, 2010). The oligopeptide transporters OPT1 and OPT4 are heterozygous, distinguishable by HindIII and EcoRI restriction

polymorphisms respectively. The efflux pump CDR2 is heterozygous with alleles encoding pumps of different drug transport efficiencies (Holmes *et al.*, 2006). The adhesin ALS3 is heterozygous with alleles containing different tandem repeat copy numbers that mediate different host cell adhesion capacities (Zhao *et al.*, 2003). The candidalysin precursor ECE1 (chromosome 4) is heterozygous with divergent 5' intergenic regions between alleles A and B, implying differential transcriptional regulation (Garbe, E., *et al.* 2023). The master regulator ROB1 is heterozygous in SC5314 with alleles differing by a single nucleotide polymorphism at position 946: the 946P allele establishes a commensal state in mouse oropharyngeal infection models while the 946S allele drives invasive behavior (Glazier *et al.*, 2023). The same cell contains both regulatory programs; the aggregate phenotype is the population-level integration of cells executing the two in different ratios.

The MTL locus, the canonical example of ancestral heterozygosity, is retained as MTLa/MTLα in approximately 97% of wild clinical isolates (Lockhart *et al.*, 2002), with homozygosis at this locus required for the parasexual mating cycle (Section 3).

Nine of ten well-characterized signaling and effector genes are heterozygous with functionally divergent alleles. The single exception is the input sensor. This is not a random distribution; it is an architectural feature. The framework implication is that the hybrid substrate has been organized across evolutionary time by selection acting on function. Components that require precise calibration to host physiological reference points are fixed by LOH to a single optimized version. Components that produce combinatorial outputs — proteolytic toolkits, toxin variants, adhesins with variable binding preferences, efflux pumps with different substrate specificities, regulatory factors with different phenotypic consequences — are retained heterozygous, so that every cell runs two versions of the output program in parallel and the aggregate population realizes an exhaustive search across the combinatorial output space.

This architecture is what enables the organism to function as a distributed biochemical computer rather than as a generic opportunist. Reference signals are unambiguous. Output responses are combinatorial. The heterozygous blocks are the parallel program substrate; the LOH regions are the committed reference modules. The white-opaque switch, chromatin-level bet-hedging, and mitochondrial methylation described in later sections operate on top of this substrate, not independently of it. The genome-wide testability of this architecture is formalized as Prediction 2a in Section 5.1. [*Stay tuned for testable predictions in §5.1.*]

To state this architecture in plain terms: the organism carries precisely calibrated instruments for reading the host and combinatorial/variable tools for responding. Think of a workshop. The measuring tools — rulers, calipers, scales — must be calibrated to a single standard; drift in the measurement renders every subsequent operation unreliable. The working tools — saws, drills, clamps — benefit from having variants on hand. A workshop with one accurate ruler and ten different saws can build a thousand different things; a workshop with ten different rulers cannot build reliably at all. *C. albicans* is organized on this principle. The glucose sensor is fixed at one version because a drifting reference would compromise every downstream decision. The response toolkit — proteases, adhesins, toxin precursors, efflux pumps, master regulators — is kept in two versions per cell, both expressed simultaneously. A single cell runs two slightly different response programs in parallel. A colony of a billion cells runs every combination of those programs at once, with host conditions selecting which combinations propagate. This is not a metaphor for computation. It is what distributed biological computation looks like at the molecular level.

3. Parasexual Reproduction & Bet-Hedging

Candida albicans reproduces by budding (clonal) or parasexuality (genetic mixing without meiosis). Parasexuality follows the opaque switch: opposite mating types fuse to a tetraploid that undergoes chromosome loss and mitotic recombination, generating genetic mosaics with novel traits including filamentation, drug resistance, and invasion (Mishra *et al.*, 2021).

The process is stress-gated (low oxygen, glucose depletion, pH, CO_2, antifungals). Frequency can rise to 10–20% under anaerobic or glucose-depleted conditions that mimic host niches; glucose depletion can even bypass the opaque step entirely (Guan, Tao, Li, *et al.*, 2023). This is a controlled subroutine for diversity generation when conditions deteriorate. The resulting variation functions as bet-hedging: different cells run different transcriptional programs, increasing population survival across micro-niches. Parasexual recombination further refines signaling efficiency, creating feedback between diversity and computational adaptability.

4. Biochemical Computer Architecture

4.0 Morphological State-Space

The biochemical computer architecture developed in this section operates through coordinated transitions between distinct morphological states. Each state is not a single morphology but an integrated cellular program with characteristic cell wall composition, surface protein expression, vesicle cargo, metabolic configuration, and immune signature. The operational outputs the organism produces — the integration of inputs into adaptive responses — manifest as transitions between these states. A reader unfamiliar with the morphological state-space will find the architectural arguments in §4.1 through §4.7 difficult to follow without the vocabulary established here.

Yeast form (blastospore). Single oval cells reproducing by budding. The commensal default at most colonization sites. Cell wall predominantly β-glucan with surface mannan layer. Slower division rate than hyphae, lower vesicle cargo diversity, immune signature consistent with regulated commensal density. Diagnostic and surveillance literature is calibrated primarily to this form, which contributes to the detection-methodology bias developed in §6 Counter-Argument 5 and (Craddock, Pan-Mammalian).

True hyphae. Continuous filamentous growth without septal constrictions. Tissue-invasive through turgor-driven tip extension. Cell wall composition shifts toward exposed β-1,3-glucan with reduced mannan masking, producing distinct pattern recognition receptor engagement. Hyphal-form extracellular vesicles carry six-fold greater protein diversity than yeast-form vesicles (Section 5.5b in Saline Oscillation), including the candidalysin-bearing payload responsible for tissue remodeling. Hyphae perform galvanotropism and thigmotropism, orienting directionally within tissue using electrical-gradient and surface-topographic cues (§4.1). Hyphae are the form that traverses the interstitium and reaches distal sites, including the cavernous sinus and pituitary region documented in §4.7.

Pseudohyphae. Chains of elongated cells with septal constrictions, intermediate between yeast and true hyphae. Often induced by nutrient stress or temperature shift. Architectural status as a partial-program state rather than a fully committed transition.

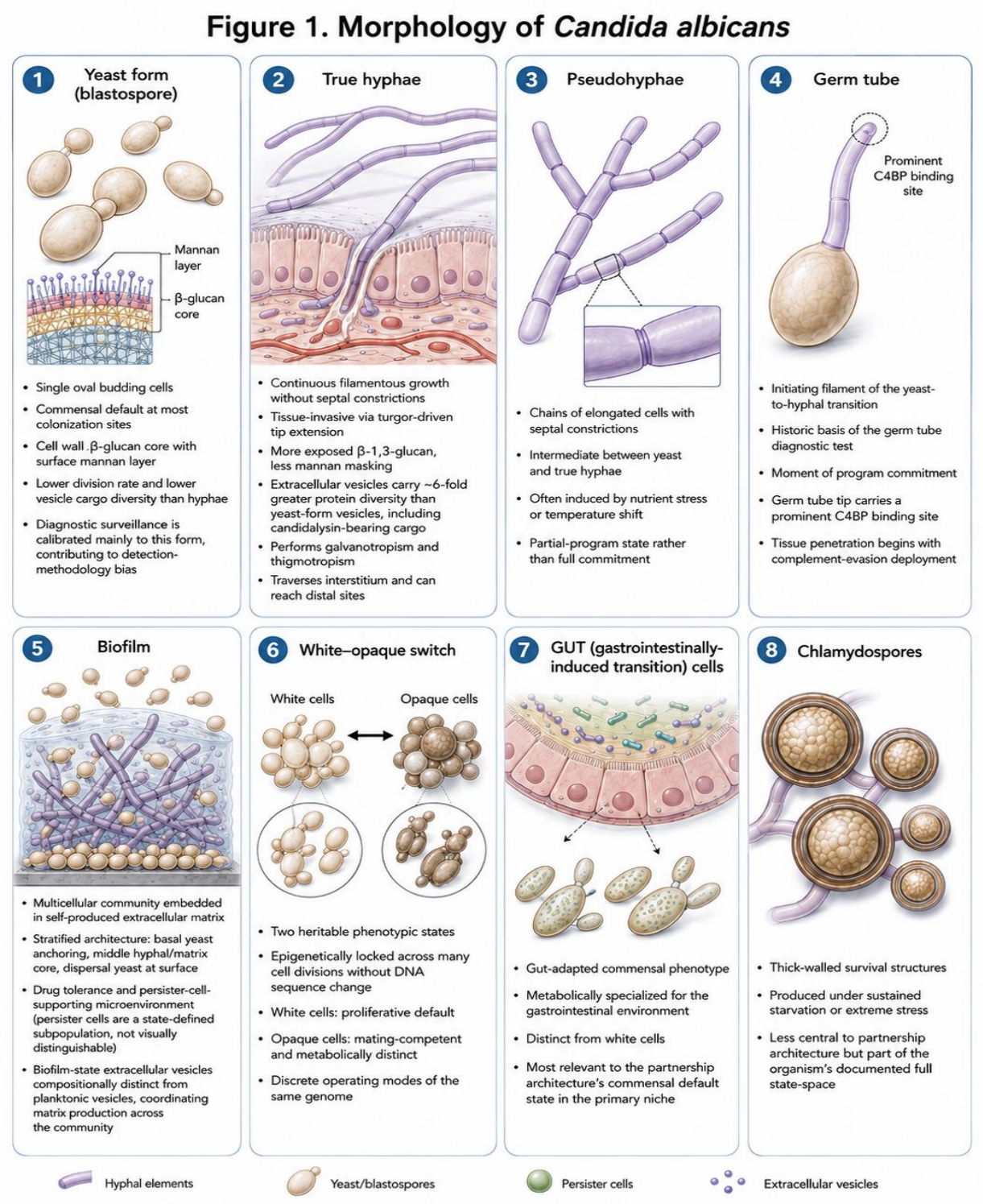


Figure 1. Morphological state-space of Candida albicans. The biochemical computer architecture developed in §4.1 through §4.7 operates through coordinated transitions between distinct morphological states. Each panel presents one form or state with its defining structural features and architectural significance. Panels 1-4 cover single-cell and transitional morphologies (yeast, true hyphae, pseudohyphae, germ tube). Panel 5 covers the population-level biofilm state. Panels 6-7 cover the heritable phenotypic states (white-opaque switch, GUT cells). Panel 8 covers the stress-survival structure (chlamydospores). The transitions between these states are not random; they are the operational outputs of the integration architecture developed in §4.2

Germ tube. The initiating filament emerging from a yeast cell at the start of the yeast-to-hyphal transition. Historically a diagnostic feature (germ tube test); architecturally the moment of program commitment. The germ tube tip carries the prominent C4BP binding site referenced in §4.3 — the moment of tissue penetration is also the moment of complement evasion architecture deployment.

Biofilm. Multi-cellular community with self-produced extracellular matrix, drug tolerance, and persister-cell-supporting microenvironment. Architecturally a population-level state distinct from individual yeast or hyphal morphology. Biofilm-state extracellular vesicles are compositionally distinct from planktonic vesicles and coordinate matrix production across the community (§4.3, §4.5). Persister cells within biofilms execute the stress-state integration architecture developed in §4.2.

White-opaque switch. Two heritable phenotypic states, epigenetically locked across thousands of cell divisions without DNA sequence change. White cells are the proliferative default; opaque cells are mating-competent and metabolically distinct. Each state is a discrete operating mode of the same genome (§4.4).

GUT (gastrointestinally-induced transition) cells. Gut-adapted commensal phenotype with metabolic specialization for the gut environment, distinct from white cells. Architecturally, the form most relevant to the partnership architecture's commensal default state in the framework's primary niche.

Chlamydospores. Thick-walled survival structures produced under sustained starvation or extreme stress. Less directly relevant to the partnership architecture but worth noting as a documented part of the organism's full state-space.

The transitions between these states are not random. They are the operational outputs of the integration architecture developed in §4.2. Yeast-to-hyphal transition, white-to-opaque switching, planktonic-to-biofilm transition — each is a state-machine transition driven by specific input combinations integrated through the convergence nodes the biochemical computer claim describes. The remainder of §4 develops how those integrations produce the morphological transitions catalogued here."

4.1 Inputs

Ten dedicated peptide transporters (two PTR and eight OPT family members; Dunkel *et al.*, 2013) import host-derived peptides as nitrogen sources and environmental sensors. A muscarinic-like cholinergic receptor senses acetylcholine (Nile *et al.*, 2018); Hgt4 is calibrated to human serum glucose (~5 mM; Brown *et al.*, 2006); additional sensors detect pH, ions, oxygen, and CO_2.

A separate input layer operates at the polarity-decision level. *C. albicans* hyphae perform galvanotropism — directional growth in response to imposed electrical fields — and thigmotropism — directional growth in response to surface topography (Brand *et al.*, 2008). They actively penetrate semi-solid substrates through turgor-driven tip extension. The same internal polarity landmark protein, Rsr1 (a Ras-like GTPase), coordinates all three responses; Rsr1 deletion attenuates galvanotropism, thigmotropism, and substrate penetration simultaneously. The mechanism is calcium-dependent: localized Ca^{2+} influx at sites of polarized growth, gated by channels activated by the appropriate environmental signal, drives the

directional output (Brand *et al.*, 2007). The galvanotropic capability means the organism reads the host's electrical-gradient landscape and orients within it — a sensing modality directly relevant to the ionic-environment co-evolutionary framework developed in the companion manuscript.

Rsr1 occupies the architectural slot for directional decisions that Cyr1 occupies for metabolic decisions (§4.2). The pattern repeats: multiple qualitatively different external cues — electrical field, surface topography, mechanical resistance — converge on a single internal coordinator that reads them through a shared second-messenger system. The organism runs two parallel second-messenger architectures simultaneously: cAMP-PKA for metabolic-state-driven morphogenesis, Ca^{2+} for environmentally-cued directional growth. Two integration nodes, two second messengers, one cell.

[*The metabolic decision and the directional decision happen at the same time, in the same cell, on the same chromatin substrate, but through separate signaling architectures. The biochemical computer is parallel, not serial. One big happy bioelectric family*]

4.2 Integration & Processing

Secreted aspartyl proteases (SAP1–10) digest host proteins. Authentic prostaglandin E_2 is produced from host arachidonic acid via divergent enzymes (Ole2/Fet3; Erb-Downward & Noverr, 2007), directly competing with host endocannabinoid synthesis (Acharya *et al.*, 2017). Extracellular vesicles carry morphology-dependent cargo including proteins, proteasome components, and RNA (Zarnowski *et al.*, 2018).

C. albicans modulates host tryptophan metabolism through the kynurenine pathway. The organism produces enzymes that divert tryptophan away from serotonin synthesis and toward kynurenine and its downstream metabolites, which suppress IL-17-mediated antifungal immunity at mucosal surfaces (Cheng *et al.*, 2010; Zelante *et al.*, 2013). This rerouting simultaneously depletes a neurotransmitter precursor and disables the host's primary mucosal defense against fungi, achieving two objectives through a single metabolic diversion. The Gpr1 receptor, primarily characterized as a carbon source sensor through Gpa2-coupled cAMP-PKA signaling, also responds to the antipsychotic clozapine, a dopamine receptor antagonist, which inhibits morphogenesis through this pathway (Midkiff *et al.*, 2011). This pharmacological intersection places Gpr1 at a node between metabolic sensing and dopaminergic signaling, suggesting the receptor's ligand range extends into host neuroactive compound space.

The cAMP-PKA pathway emerges from these inputs as a multi-input convergence node rather than a single-stream signaling cascade. The adenylyl cyclase Cyr1 is the central integrator. Cyr1 binds CO_2/bicarbonate directly, integrating host metabolic gas tension into the cAMP signal (Hall *et al.*, 2010). Bacterial peptidoglycan also activates Cyr1 directly, providing a chemically unrelated input stream that reports the bacterial-community state of the local niche (Xu *et al.*, 2008). Farnesol, the organism's own quorum-sensing molecule, suppresses the same cAMP-PKA cascade through inhibition of Ras1 upstream of Cyr1, contributing a population-density input with opposite valence to the activating signals (Davis-Hanna *et al.*, 2008). The Gpr1 GPCR feeding into Gpa2-coupled cAMP signaling adds an additional input class — lactate from immune-cell glycolytic burst, methionine from biosynthetic activity, dopaminergic ligand space — through a parallel upstream branch.

Multiple qualitatively different input classes feed the cAMP-PKA decision node: host metabolic gas, bacterial neighbor signal, organism population-density signal, and host-

physiology signals routed through Gpr1. The signals do not all act on the same molecule — CO_2 and peptidoglycan engage Cyr1 directly, farnesol acts upstream through Ras1, Gpr1 feeds in via Gpa2 — but they all converge on the cAMP concentration that PKA reads to drive morphogenetic output. The cAMP level is the integrated arithmetic. The signature is computational: not a sensor reading a single input, but an integration node summing multiple weighted inputs of mixed valence into a single decision variable. [*Cyr1 is not the sensor. It is where the sensors meet.*]

The same integration architecture operates under antifungal pressure to produce persister cells — quiescent subpopulations within biofilms that survive drug exposure through coordinated activation of drug efflux (CDR1/CDR2, MDR1), ergosterol biosynthesis (ERG11/ERG3/ERG5), oxidative stress resistance (SOD1/SOD2), HOG-MAPK signaling, cell wall remodeling, and heat shock protein deployment, with concurrent shift to glycolytic metabolism and reduced ATP (Wu et al., 2026).

Figure 2 Three Parallel Integration Architectures and Coordinated System Outputs

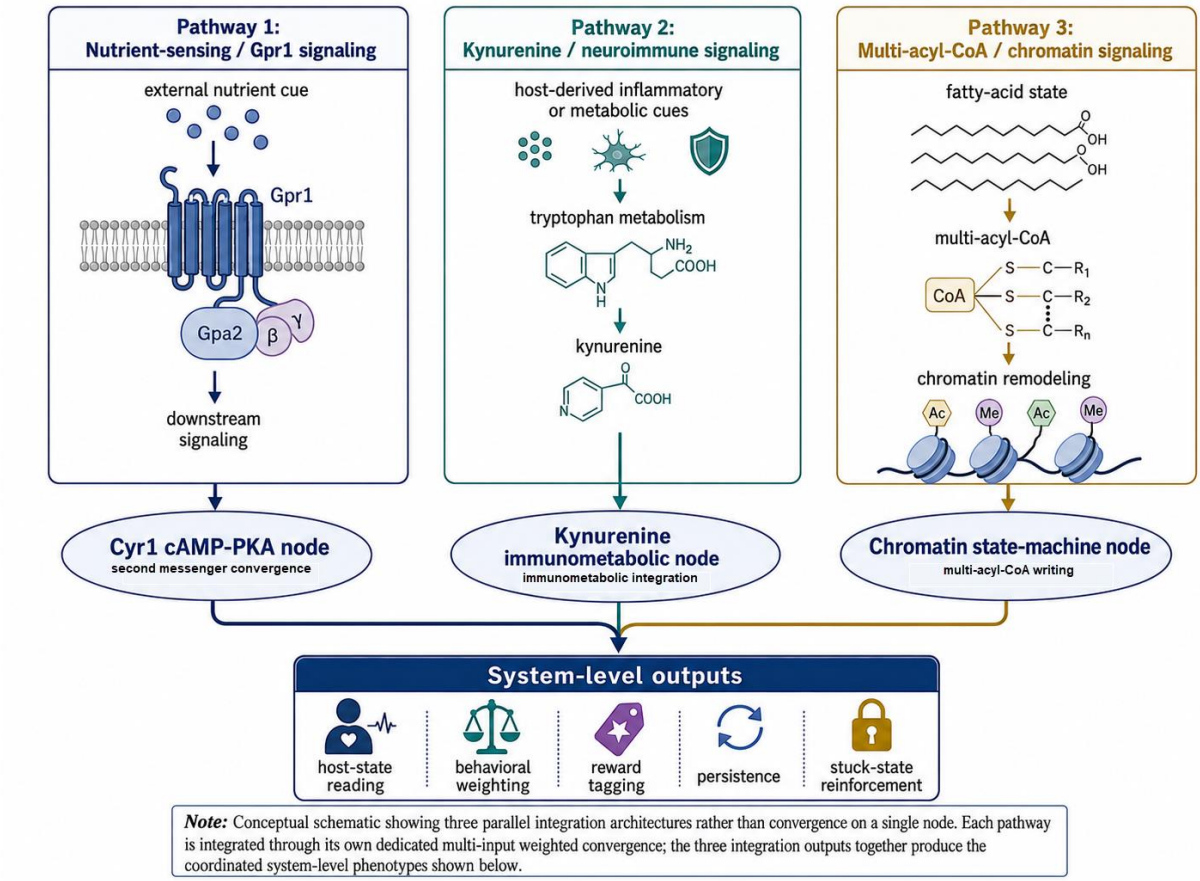


Figure 2. Three parallel integration architectures from Paper A's distributed biochemical computer model. Pathway 1 — Gpr1/Gpa2 nutrient-sensing converging at the Cyr1 cAMP-PKA decision node (§4.1, §4.2). Pathway 2 — host-derived inflammatory and metabolic cues processed through tryptophan-kynurenine immunometabolic integration (§4.2, §4.3). Pathway 3 — fatty-acid-state inputs written into chromatin via the multi-acyl-CoA panel and read by the chromatin state-machine (§4.4). The three integration architectures operate in parallel rather than feeding a single common node; together they produce the coordinated system-level phenotypes the framework predicts. Some outputs map onto material developed more fully in companion framework papers (reward tagging and stuck-state reinforcement). The user does not act on these integration nodes directly, but on the host systems whose state the organism reads.

Six independent biological systems coordinate into a single stress-survival state. The mainstream reading frames persister cells as a treatment-resistance problem; the framework

reads them as the stress-state expression of the same multi-pathway integration architecture that operates at lower pressure for commensal/morphogenetic decision-making.

4.3 Outputs

Yeast-to-hyphal transition, immune modulation (Th2 shift via PGE_2, dendritic cell suppression via farnesol, LILR engagement via Ece1-II and Ece1-V peptides), tissue remodeling (candidalysin pores, EGFR ubiquitination/lysosomal degradation, and CCNH binding that inhibits DNA damage repair; Lin *et al.*, 2024; Moyes *et al.*, 2016), bidirectional pH engineering (Vylkova *et al.*, 2011), and endocannabinoid tone modulation. The alkalinization machinery that drives the active-modification arm of pH engineering — Stp2p-regulated amino acid permease expression, Csh3p-mediated permease folding, Dur1,2p urea amidolyase activity converting urea to ammonia, and Ato-family ammonia export significantly expanded in *C. albicans* relative to non-alkalinizing species — operates independently of the canonical Rim101p pH adaptation pathway (Vylkova *et al.*, 2011). Two parallel regulatory architectures coexist in the same cell: Rim101p for adaptation to ambient pH, and the Stp2p-Ato system for active modification of ambient pH. This is the structural signature the biochemical computer claim requires — dedicated machinery for environmental control distinct from environmental sensing.

The endocannabinoid tone modulation described above has a specific downstream consequence in autonomic nervous system governance. The organism accesses the parasympathetic arm directly through its documented muscarinic-like cholinergic receptor (Section 4.1; Nile *et al.*, 2018), which senses acetylcholine as a host-state input. The sympathetic arm presents a different architecture. Wurster *et al.* (2021) tested epinephrine and norepinephrine directly against *C. albicans in vitro* and found no significant effect on growth, morphology, or virulence factor expression. The organism does not sense catecholamines. It does not need to. CB1 receptor activation at pre-synaptic sympathetic nerve terminals inhibits norepinephrine release (Schlicker & Kathmann, 2001). By modulating endocannabinoid tone through the arachidonic acid competition described above, the organism governs the rate of norepinephrine release without sensing the molecule itself. This is indirect governance of a system whose direct input the organism cannot read: it controls the faucet rather than measuring the output. The pharmacological confirmation is guanfacine, an alpha-2 adrenergic agonist that reduces norepinephrine release through a parallel pre-synaptic mechanism. Guanfacine replicates pharmacologically what the organism achieves through ECS modulation of the same nerve terminals, and its clinical efficacy in reducing hyperactive sympathetic tone is consistent with the prediction that ungoverned or undergoverned sympathetic output is the baseline state when organism ECS governance is absent or disrupted. The clinical phenotype of disrupted ECS governance at this control point — sympathetic output without a corresponding brake, particularly in the splanchnic bed — is examined in a forthcoming Architect Report on chronic insufficient venous return. [*The parasympathetic gets read directly. The sympathetic gets governed at the faucet. The organism does not need to measure what it is already controlling.*]

Cell wall components provide an additional immune output channel. Alpha-mannan and beta-glucan surface structures trigger mast cell degranulation and stimulate arachidonic acid release from host macrophages via mannose and beta-glucan receptor engagement (Castro *et al.*, 1994). This is distinct from the prostaglandin, farnesol, candidalysin, and LILR-mediated immune mechanisms described above: it operates through innate pattern recognition receptors rather than secreted metabolites, and the degranulation response activates downstream

inflammatory cascades (histamine, proteases, cytokines) that the organism's other immunomodulatory outputs then redirect toward the non-protective Th2 profile.

The organism captures host complement regulators on its surface to evade complement-mediated killing. Both yeast and hyphal forms bind C4b-binding protein (C4BP, the classical and lectin pathway inhibitor), with a prominent binding site at the germ tube tip — the structure responsible for tissue penetration (Meri *et al.*, 2004). Surface-bound C4BP retains its regulatory activity, inactivating C4b at the fungal surface and suppressing classical-pathway complement activation. The same fungal surface simultaneously binds factor H and FHL-1, the alternative-pathway regulators. *C. albicans* therefore captures regulators of all three complement pathways and presents them as host-marked surface coverage that the complement system reads as self. Multiple fungal surface proteins mediate this capture: Pra1 (pH-regulated antigen 1) binds C4BP, factor H, FHL-1, and plasminogen (Luo *et al.*, 2010); Hgt1p (high-affinity glucose transporter 1) doubles as a multifunctional complement evasion molecule, binding both Factor H and C4b-binding protein and comprehensively interfering with all three complement activation pathways (Lesiak-Markowicz et al., 2011; Harpf et al., 2020). The same fungal proteins that handle metabolism and surface chemistry moonlight as complement-regulator capture devices, and the surface-attached C4BP additionally mediates adhesion to host endothelial cells, converting an immune-evasion event into a tissue-attachment event in a single binding interaction. [The fungal surface wears the host's own regulators as a borrowed uniform. The complement system reads the uniform and stands down. No alarms go off.]

Host metabolic state is an additional output layer. *C. albicans* colonization produces a 4-to-6-fold reduction in plasma leptin in high-fat-diet murine models and shifts the leptin/ghrelin ratio toward sustained appetite signaling (Peroumal *et al.*, 2022; Gutierrez *et al.*, 2025). The organism has no leptin receptor, produces no leptin-mimetic metabolite, and does not sense leptin directly. It alters host leptin through colonization-driven effects on adipose signaling, vagal tone, and microbiota composition — writing a metabolic-state signal into the host without reading it. The same output class is evident in lipoprotein metabolism: intestinal *C. albicans* secretes formyl-methionine, which activates intestinal HIF-2α, induces ceramide biosynthesis, and elevates host LDL-C and total cholesterol in dyslipidemia patients and mouse models, reversible by the HIF-2α antagonist PT2385 (Wang *et al.*, 2024). The same parameter responds in the opposite direction under antifungal pressure: chronic high-dose ketoconazole reduces LDL-C by 10–41% in dose-dependent fashion across published clinical series (Lionakis *et al.*, 2008), and the inverse arrow makes the bidirectional governance signature explicit — organism activity elevates the parameter, antifungal-mediated organism reduction collapses it. Formyl-methionine is a conserved fungal metabolite; HIF-2α is a host transcription factor; the pathway is a clean metabolite-to-transcription-factor write operation. Together, leptin suppression and LDL-C elevation constitute a coordinated host metabolic-state output channel operating through two non-overlapping molecular pathways. Both outputs are measurable in routine human clinical chemistry and scale with colonization density, making this the most clinically accessible of the organism's output layers. The host's apolipoprotein B carries embedded antifungal cryptides (r(P)ApoBLPro, r(P)ApoBLAla, r(P)ApoBSPro, (Dell-Olmo *et al.*, 2021) that localize to the fungal surface and induce membrane damage against *C. albicans* — indicating that the principal structural protein of host LDL has been under selection for anti-*Candida* activity. The organism raises the level of a host lipoprotein whose carrier protein contains sequences designed to kill it. This is the coevolutionary signature the committed-input / parallel-output architecture predicts at the metabolic interface: both arrows of a long negotiation visible in a single protein family.

A second host serum protein follows the same dual-function architecture. Hepcidin, the hepatic peptide hormone that governs systemic iron homeostasis through ferroportin internalization, is essential for resistance to disseminated candidiasis. Genetic and inducible hepcidin knockout mice show unrestrained fungal growth and increased yeast-to-hypha transition with exposed β-1,3-glucan, exacerbating kidney injury independently of candidalysin (Arekar *et al.*, 2025). Therapeutic administration of the hepcidin mimetic PR-73 improves outcomes in the same model. The mechanism extends beyond iron sequestration: hepcidin-25 directly induces apoptosis in *C. albicans* through antimicrobial peptide activity (Chen and Lan, 2020). Like apolipoprotein B, hepcidin is a host serum protein with two functions selected against the organism — a regulatory hormonal function (iron restriction) and a direct cidal function (AMP-mediated fungal apoptosis). The chronic-liver-disease → low-hepcidin → candidemia pathway documented in critically ill patients is the clinical signature of this counter-measure failing when its production is impaired.

The organism's iron-acquisition machinery is the parallel-output toolkit responding to host iron restriction: high-affinity iron permeases Ftr1 and Ftr2, the heme-acquisition cell-surface protein Rbt5, siderophore uptake systems, and reductive iron acquisition through Cfl-family ferric reductases. *C. albicans* deploys multiple iron-acquisition routes simultaneously, with the operational route depending on which host iron pool remains accessible. Hepcidin sufficiency restricts the pool the organism can reach; hepcidin insufficiency releases it. The interface is a measurable arms race: host hepcidin levels are clinically assayable, organism iron-acquisition expression is detectable in clinical isolates, and the pharmacological lever (PR-73 and emerging hepcidin mimetics) is in active therapeutic development.

[ApoB carries cryptides that kill the organism at its surface. Hepcidin starves it and kills it directly. The host serum proteome carries the negotiation history. So much for the ApoB suppressors.]

Bile acid signaling represents a third write operation in the same architectural class. *C. albicans* does not produce bile acids and has no characterized FXR ligand among its secreted metabolites. However, CA expansion correlates with depletion of the commensal bacteria responsible for taurocholic acid (TCA) deconjugation and dihydroxylation — Lactobacillus johnsonii, Turicibacter sanguinis, and Clostridium celatum (Thangamani *et al.*, 2021). Loss of these deconjugators produces TCA accumulation in the cecum and colon. TCA absorbed via the apical sodium-dependent bile acid transporter (Slc10a2/ASBT) binds the farnesoid X receptor (FXR), and this binding produces a coordinated host transcriptional shift — antifungal peptide ang4 down, antifungal macrophage receptor CX3CR1 down, tight junction protein ZO-1 down — that is permissive for further CA expansion. The loop is self-reinforcing: TCA at 1% in drinking water alone, without antibiotics or immunosuppression, is sufficient to drive CA colonization and dissemination in wild-type mice (Thangamani *et al.*, 2021). As with leptin and LDL-C, the organism shapes a host signaling axis without binding its primary mediator. Unlike those cases, the bile acid loop has measurable intermediate species at every step and is the most clinically accessible of the three for diagnostic application.

Bidirectional cross-kingdom communication has now been documented at the molecular detail level. Halder et al. (2022) showed that human monocytes encountering C. albicans release extracellular vesicles containing the human microRNA hsa-miR-24-3p, that this miRNA crosses the kingdom boundary and enters fungal cells, and that inside the fungal cell it suppresses translation of the fungal cell-cycle brake Sol1, promoting fungal cell division. The packaging of this host-derived cargo into vesicles is triggered by fungal β-glucan binding to host CR3 and

fungal mannan binding to host TLR4 — the same molecular interactions the standard model categorizes as host pattern recognition of fungal pathogen-associated molecular patterns. The receptor-ligand binding events that mainstream framing reads as host detection of pathogen are simultaneously the docking events that license host-side cargo packaging across the kingdom boundary. The host's response to the organism is not only complement and immune attack; it includes packaged cargo that promotes organism cell division. The architectural significance is that host-organism communication operates bidirectionally through the same molecular interfaces, consistent with the partnership architecture predicted by 200 million years of co-evolution. [*The standard model calls these molecules pattern recognition receptors detecting pathogens. The same molecules license the host to send growth-promoting cargo across the kingdom boundary. Both readings can be accurate. Selection ran on what the molecules do, not on what we labeled them.*]

4.4 Memory & State Maintenance

White-opaque phenotypic switching is epigenetically heritable across thousands of cell divisions without DNA sequence change, stabilized by histone modifiers (Sir2, Hda1, Hda2/3) that lock transcriptional states (Lohse *et al.*, 2009; Qasim *et al.*, 2021).

Beyond the white-opaque switch, the organism's epigenetic architecture includes additional layers. Chromatin modifications, specifically histone methylation and acetylation patterns, regulate the commensal-to-pathogen transition and provide the mechanistic basis for the transcriptomic heterogeneity observed across genetically identical populations (Dumeaux *et al.*, 2023; Mishra *et al.*, 2011). Mitochondrial genome methylation represents a further regulatory layer governing energy metabolism (Bartelli *et al.*, 2018). These modifications are fast and reversible compared to genetic mutation, enabling rapid phenotypic switching across the population without altering the underlying genome. The result is a memory system operating at multiple timescales: white-opaque locking for long-term state maintenance, chromatin-level switching for medium-term niche adaptation, and mitochondrial epigenetic tuning for metabolic responsiveness.

The chromatin state-machine architecture introduced here operates as the substrate on which the signaling-level integration described in the preceding three sections on inputs, memory and state maintenance, and outputs. The biochemical computer claim refers to the integrated multi-layer system, not to chromatin or signaling alone. Inputs are committed at genome level (§2.2), states are inscribed at chromatin level (this section), and integration outputs are produced at signaling level. The morphological transitions catalogued in the section on morphological state-space are the visible expressions of state changes inscribed in chromatin and triggered by signaling integration. The 'computer' is the assembled system, not any individual layer.

IV.IV.I Chromatin State-Machine Architecture

A note on analogy before the architectural detail. Computer architecture vocabulary — read-only memory, working memory, processor, firmware — invites itself into discussions of distributed biological information processing because the engineering categories are familiar and the biological categories are not. The invitation should be declined, not because the comparison is wrong in spirit, but because the engineering categories carry assumptions the biology does not satisfy. In a computer, the processor is a distinct component from memory; firmware in ROM is read by a CPU that is architecturally separate; working data in RAM is held in physically

different hardware than the instructions executing on it. *C. albicans* does not respect that separation. The chromatin substrate stores state and participates in executing transitions. The same histone modifications that record metabolic configuration recruit and exclude the transcription factors that read those modifications and act on them. There is no separate processor reading the marks. The marks are part of the reading apparatus.

This is what 200 million years of mammalian co-evolution produced — an architecture in which storage, processing, sensing, and output are interwoven rather than partitioned. The organism is not sentient, does not think, and runs no program in the directed-execution sense. It runs distributed chemical computation on a substrate that engineering has not built and may not have vocabulary for. That gap is the reason this paper reaches for analogy at all: not because the analogies fit, but because without them, no reader carries away anything but a list of capabilities. The biochemical computer framing is the closest available shorthand for an information-processing system that operates outside the architectural categories most readers know. The analogies in this paper — committed-input parallel-output, multi-input convergence, state-machine substrate — are scaffolding to the mechanism, not claims about what the mechanism is. The mechanism is the chromatin and the metabolites and the proteins doing what they do. The analogies exist because the alternative is leaving the reader with no handhold at all. [*Two hundred million years built something engineering hasn't. The analogies are how we point at it. Maybe we can design a more similar "computer" in the future.*]

The mechanisms described in the preceding opening, maintain heritable phenotypic states. They are storage. State-machine operations — the transitions between operational modes the organism executes in response to host conditions — run on a separate chromatin substrate using writer, reader, and eraser hardware that reads metabolic-state inputs and writes them into transcriptional output. The vocabulary is not metaphor. The proteome-wide post-translational modification architecture this requires has been measured in *C. albicans* directly.

Quantitative analysis of the *C. albicans* crotonylome by anti-crotonyl antibody enrichment with LC-MS/MS identified 5,242 lysine crotonylation sites distributed across 1,584 proteins, accounting for 17.5% of the entire proteome (Zhou *et al.*, 2021). Combined with previously characterized acetylation and succinylation profiles in the same strain, the proteome-wide PTM architecture concentrates on biosynthetic enzymes, ribosomal biogenesis, oxidative phosphorylation, nuclear activity, and proteasome formation — exactly the cellular machinery whose throughput must adjust to changing host conditions. The same writer-family enzymes (p300/CBP-family) deposit acetyl, succinyl, propionyl, butyryl, and crotonyl marks; sirtuin-family erasers remove them. One writer-reader-eraser hardware system reads multiple distinct metabolic-state inputs simultaneously, because each acyl-CoA species reflects a different metabolic configuration: acetyl-CoA from glycolytic flux, succinyl-CoA from TCA cycle activity, crotonyl-CoA from short-chain fatty acid β-oxidation and from lysine and tryptophan catabolism. The organism's current metabolic configuration is continuously inscribed into its chromatin via this multi-acyl-CoA panel, and the same chromatin substrate is read out as transcriptional decisions about which programs to run. [*Multi-acyl-CoA chromatin modification means the organism's metabolic state is not just metabolized. It is encoded.*]

Genetic disruption of single chromatin enzymes confirms the architectural role. Deletion of GCN5, encoding a paradigm lysyl-acetyltransferase, abolishes virulence in a tail-vein mouse infection model with full clearance of systemic infection (Shivarathri *et al.*, 2019). The mechanism is not a single pathway: gcn5Δ/Δ cells fail to filament normally, show inverted FKS1/FKS2/FKS3 expression that produces caspofungin hypersusceptibility, exhibit differential

phosphorylation of three independent MAPK pathways (Mkc1, Cek1, Hog1), lose Efg1-mediated ALS1 induction with collapse of polystyrene adhesion, fail to induce SOD5 under caspofungin challenge, and become hypersensitive to macrophage killing. One acetyltransferase coordinates morphogenesis, cell wall architecture, three MAPK signaling pathways, adhesion, oxidative stress response, iron homeostasis, drug efflux, and macrophage survival. The chromatin enzyme is not modulating one program. It is enabling the integrated virulence program to run at all. [*Same protein. Different chromatin context. The protein doesn't change. The substrate it tries to bind has changed what it accepts.*]

The hyphal repressor Nrg1 illustrates how the same protein produces opposite functional outputs depending on chromatin context. Nrg1 represses hyphal genes in yeast-form cells. During hyphal initiation, NRG1 mRNA is cleared. During hyphal maintenance, Nrg1 protein is re-expressed but excluded from its target promoters by Hda1-mediated deacetylation of Tup1 partner factors (Lu *et al.*, 2011, 2014). Same protein, opposite functional output, determined by the chromatin context the protein encounters at the promoter. This is a chromatin-gated repressor element: the chromatin landscape determines whether protein-level inputs translate into transcriptional output.

A clade-specific chromatin innovation provides architectural insight into how the organism balances commensal and pathogenic states. The variant histone H3 (H3V^CTG^), exclusive to the CTG clade of ascomycetes including *C. albicans* and absent from all other ascomycetous fungi analyzed, occupies promoters of biofilm-related genes preferentially in planktonic cells (Rai *et al.*, 2019). Three amino acid changes from canonical H3 — at positions 31, 32, and 80 — define the variant; site-directed mutation establishes that positions 31 and 32 in combination are necessary and sufficient for biofilm-repression function. The mechanism is biased eviction: during the planktonic-to-biofilm transition, H3V^CTG^ nucleosomes are selectively evicted from biofilm gene promoters, opening chromatin access to the biofilm master regulators Bcr1, Tec1, and Ndt80, while canonical H3 occupancy remains unchanged (Brahma *et al.*, 2023). The histone chaperone CAF-1, not HIRA, loads H3V^CTG^ (Singha *et al.*, 2023). Two findings sharpen the architectural reading. First, H3V^CTG^ and canonical H3 form heterotypic nucleosomes — one variant plus one canonical H3 in the same octamer — providing a graded rather than binary chromatin landscape over biofilm gene promoters. Second, deletion of H3V^CTG^ rescues biofilm defects in three master regulator knockouts (bcr1, tec1, ndt80 single mutants), establishing that the chromatin gate operates beneath the master-TF layer: removing the chromatin restriction can compensate for loss of the regulators that normally open it. [This is a single-celled organism being told what the properties of its outer barrier will be by chromatin encoding. Think of it as a continuously running 3D printer]. The variant exists across CTG-clade members, including non-mammal-colonizing species; functional characterization has been performed in *C. albicans* only. The biofilm-balancing function operates on a substrate — mammalian-host biofilm formation — that does not exist for the non-mammal-colonizing CTG-clade members. Clade-shared hardware deployed in mammal-colonization context, with the within-clade functional comparison untested.

H3V^CTG^ is not the clade's only chromatin innovation. CTG-clade-specific protein components of the RSC chromatin-remodeling complex regulate cell-cycle progression in *C. albicans* ([Authors], 2026, mSphere; DOI 10.1128/msphere.00084-26). Two independent clade-specific chromatin-level adaptations — a variant histone and variant remodeler subunits — operate in parallel on the same chromatin substrate. The pattern indicates chromatin is the primary substrate for clade-specific functional specialization, not a peripheral one.

The chromatin layer surfaces a candidate convergence point with host chromatin biology. The active-promoter mark H3K4me3 is deposited by Set1/COMPASS in *C. albicans* and by SET1A/SET1B/MLL1-4 in mammals. The writer family is deeply conserved across eukaryotes; the mark itself is identical. SETD1A loss-of-function variants are an established schizophrenia risk factor (Singh *et al.*, 2016, Nat Genet). Shared mark and shared writer architecture establish a candidate convergence point worth specific investigation — not a demonstrated cross-kingdom channel. A channel would require a mechanism by which organism state influences host SETD1A activity or vice versa: extracellular vesicle delivery of chromatin modifiers, organism-derived metabolites constraining one-carbon metabolism and SAM availability, or specific organism-derived inhibitors of SETD1A. None has been demonstrated. The convergence point flags this axis for future evaluation.

The chromatin state-machine layer is therefore a multi-input, multi-acyl-CoA, clade-specialized substrate that integrates organism metabolic state, environmental cues, and master-regulator activity into transcriptional decisions about which program to run. It operates beneath the 4.1input layer, the 4.2 integration layer, and the 4.3 output layer, providing the substrate on which those layers are inscribed. The memory layer, IV.IV, records states the state-machine has executed; the chromatin state-machine layer executes the transitions. [*The chromatin is not where memory is stored. It is where decisions are made. The master regulators carry keys to a lock the variant histone closes, configuring the program, the metabolic state writes itself onto the substrate that decides what runs next, and the clade specialized this layer first because this is the layer that runs the show. This is our single-celled organism.*]

4.5 Spatial Multiplexing & Feedback

Different subroutines run concurrently in distinct micro-niches (lumen glucose harvesting, invading hyphae with SAPs/alkalinization, phagosomal lactate/ketone use). Biofilm regulatory networks contain feed-forward loops that reinforce expression of key targets (e.g., via Brg1, Wor3, Ume6 reinforcing Efg1 outputs), stabilizing the network against genetic variation (Cravener *et al.*, 2023). Multi-input integration is evident in hyphal morphogenesis: pH, temperature, nutrients, CO_2, and quorum signals converge on shared pathways (cAMP-PKA, MAPK) to produce a single morphological decision (Kornitzer, 2019).

Rapid emergence of multiscale interaction networks has been observed in experimental bacteria-phage coevolution, where simple reciprocal selection in well-mixed cultures produced nested-modular cross-infection patterns in just 21 days (Borin *et al.*, 2023). “We show that multiscale network structure can evolve rapidly under simple ecological conditions without spatial structure […] illustrating Darwin’s idea that simple adaptive processes can generate entangled banks of ecological interactions.” The *Candida* biochemical computer operates with far richer input channels and output layers, yet follows the same principle: fluctuating host conditions (nutrient gradients, immune pressure, pH, perfusion) drive the rapid refinement of distributed, hierarchical subroutines across the population.

Hyphal transit through subcutaneous interstitial tissue is mechanically active rather than passive. The galvanotropism and thigmotropism documented in §4.1 establish that the organism orients directionally within tissue using electrical-field and topographic cues, with Rsr1-mediated polarity integration coordinating directed extension. Subcutaneous tissue is innervated by free nerve endings, Meissner corpuscles, and Pacinian corpuscles that respond to mechanical deformation of surrounding tissue. Directional hyphal transit through this tissue produces

deformation that activates these mechanoreceptors. The resulting sensation — discrete movement under skin, often localizable by touch, persistent during organism-active states — is termed formication and is currently classified as a psychiatric symptom (tactile hallucination, dermatozoenwahn, Ekbom syndrome) under the standard model, which has no mechanism for genuine sub-dermal movement and therefore reads the report as perceptual rather than physical.

White *et al.* (2025) document a clinical case in which formication co-occurred with destructive nasal-septum lesions and confirmed *C. albicans* tissue infection, providing direct concurrence of organism tissue presence and crawling sensation in a single peer-reviewed case. Hoss *et al.* (1998) document burning, stinging, and crawling scalp sensations as a recognized clinical entity in dermatology, present in patients without visible lesions — a phenomenon the standard model identifies as real but cannot mechanistically explain. The framework reads formication as the externally perceptible signal of an architectural feature already documented in §4.5: the organism's directional transit through the body-wide interstitial distribution network, detected by the mechanoreceptors that monitor subcutaneous tissue deformation.

A simple bedside observation distinguishes the mechanical mechanism from the perceptual one: applied finger pressure at the location of the sensation halts directional progression while motion in place continues. Hallucinations do not respond to mechanical pressure; physical entities encountering mechanical resistance do. The signature is consistent with hyphal extension blocked from forward progression while continuing local growth at the tip. The test is zero-cost, requires no equipment, and is reproducible by any person experiencing the sensation. The standard psychiatric framing has no prediction for the response to applied pressure because it does not posit anything physical to apply pressure against.

A second bedside observation reinforces the mechanical reading: topical antifungal application produces sensation reduction within twenty-four hours on asymptomatic skin overlying the reported transit zone. The kinetics — sub-day response rather than days-to-weeks pharmacological onset — are consistent with direct interaction at organism population accessible from the skin surface, not with central nervous system mechanism. Both bedside tests are within reach of any clinician or patient and both have been universally absent from the formication evaluation pathway because the standard framing has not posited a target the tests could engage. The misclassification is not a clinical disagreement but a category error: the sensation is real, the mechanism is mechanical rather than perceptual, and the standard reading inverts the diagnostic question. Patient self-report communities document the formication-during-*Candida*-flares pattern with high frequency; the medical literature does not. The detection gap is not in the patients.

[The patient feels something move. The patient puts a finger on it. The motion stops progressing but continues in place. The patient applies topical antifungal. The sensation reduces in hours. Hallucinations do not respond to fingers or to clotrimazole. The standard model has no place to put either finding because the standard model is the wrong model. Formication is the mechanoreceptor reading hyphal transit. The diagnostic apparatus has had no place to put this signal, so it has been filed under hallucination for a century. I can testify, it is not. It took me less than an hour to come up with that finger test. You can check that box.]

No other organism is known to integrate this full suite.

4.6 The Interstitium as Distribution and Signaling Infrastructure

The preceding sections describe the organism's sensing, processing, and output capabilities at the cellular and population level. This section addresses the physical medium through which the distributed computer's signals propagate and through which peripheral colonies access host resources.

The interstitium, historically treated as inert connective tissue, was recharacterized by Benias *et al.* (2018) using confocal laser endomicroscopy on living tissue. Standard histological fixation collapses the fluid-filled spaces, rendering them invisible on fixed slides. In vivo imaging revealed a body-wide network of collagen-lined, fluid-filled compartments present beneath the dermis, surrounding the gastrointestinal tract, lungs, urinary system, and vasculature. The structural continuity of these compartments across organ boundaries establishes a pre-lymphatic fluid highway that connects otherwise anatomically distinct tissue sites.

This network has three properties directly relevant to the biochemical computer model.

First, it functions as a signaling medium. Interstitial fluid carries cytokines, extracellular vesicles, damage-associated molecular patterns, and purine nucleotides between tissues. The organism's documented output channels, including extracellular vesicles with morphology-dependent cargo (Section 4.2), candidalysin-mediated ATP efflux activating purinergic receptors (Section 4.3), and prostaglandin E2 produced from host arachidonic acid (Section 4.2), are all soluble or vesicle-borne signals compatible with interstitial fluid transport. A colony at any mucosal or dermal site can broadcast signals into the interstitial network without requiring bloodstream access, reducing exposure to circulating immune surveillance.

Second, it provides a nutrient interface at the dermal boundary. The epidermis is avascular. Basal keratinocytes, the proliferative layer at the bottom of the epidermis, receive all nutrients by diffusion from dermal capillaries across the basement membrane. The interstitium interpenetrates the dermis and surrounds these capillaries. Hyphae positioned at or near the basal layer would occupy the optimal location for intercepting glucose diffusing upward from the vasculature while simultaneously accessing a continuously renewing cellular substrate (basal keratinocytes themselves). This positioning is consistent with the Hgt4 glucose sensor calibration described in Section 4.1: the organism does not need to be intravascular to sense and consume host glucose at physiological concentrations. It needs only to be at the nutrient interface where capillary-derived glucose enters avascular tissue.

Third, the interstitial compartments are mechanosensitive. Fibroblasts populating the collagen matrix express purinergic receptors (P2X, P2Y families responsive to extracellular ATP), toll-like receptors (TLR2, TLR4 recognizing fungal cell wall components including mannan and beta-glucan), and cytokine receptors. Physical compression or stretch alters fluid flow through the compartments and can activate mechanosensitive signaling cascades in resident fibroblasts. For an organism that produces candidalysin (a pore-forming peptide that causes ATP efflux from damaged host cells) and whose cell wall components trigger innate pattern recognition, the interstitial fibroblast network represents a distributed array of signal-responsive cells that the organism can activate through its normal virulence toolkit.

The interstitium therefore functions as the organism's equivalent of a bus architecture: a shared physical medium connecting distributed processing nodes (peripheral colonies at distinct anatomical sites) and enabling both nutrient access and signal propagation without dependence on the bloodstream. The spatial multiplexing described in Section 4.5, in which different subroutines run concurrently in distinct micro-niches, requires a physical substrate for inter-niche coordination. The interstitial fluid network provides it.

Topical antifungal response as indirect evidence. If peripheral colonies at the dermal nutrient interface constitute functional nodes in the distributed system, topical antifungal agents that penetrate the stratum corneum should produce measurable effects disproportionate to the surface area treated. Lipophilic azoles (miconazole, clotrimazole) are designed for epidermal penetration and would reach basal-layer colonies directly. Medium-chain fatty acids (caprylic acid C8, capric acid C10, lauric acid C12, the primary antifungal components of coconut oil) disrupt fungal cell membranes through a non-azole mechanism with no cross-resistance to ergosterol synthesis inhibitors. The combination of two azoles with different binding profiles plus MCFAs would present three independent kill mechanisms against peripheral colonies simultaneously.

The longitudinal case study (Craddock, 2022 log; Craddock, Redacted Science) documents recurrent topical antifungal use over a multi-year period, with Amazon purchase records providing third-party-timestamped evidence of treatment intensity correlating with documented symptom severity: 22 tubes purchased in the 2022 crisis year, declining to 8 tubes in 2026. The burning sensation reported during topical application, intensified by pressure against surfaces (compressing interstitial compartments and concentrating inflammatory mediators from colony die-off against sensory nerve endings), and responsive to ice (vasoconstriction reducing inflammatory mediator delivery plus direct TRPV1 inhibition), is consistent with an active colony destruction event rather than a dermatological irritation response. Healthy skin does not produce a burning inflammatory response to antifungal ointment.

Prediction (proposed as Prediction 13 or renumbered as appropriate): Topical antifungal application over defined skin areas in subjects with elevated commensal *Candida* colonization (assessed by mycobiome profiling) will produce measurable changes in local skin temperature (infrared thermography, as a proxy for altered vascular tone) and local interstitial cytokine profiles (microdialysis sampling) that scale with pre-treatment colonization density and differ between azole-class and MCFA-class agents, consistent with colony reduction at the dermal nutrient interface rather than nonspecific irritation. Subjects with low colonization density will show no such response to the same agents.

4.7 The Microadenoma as Tissue Stress Response

Pituitary microadenomas are conventionally classified as benign neoplasms of the anterior pituitary, defined as lesions smaller than 10 mm in diameter. Meta-analytic data report an overall prevalence of 16.7%, with 14.4% found in autopsy studies and 22.5% in radiological series (Ezzat *et al.*, 2004). The standard clinical interpretation treats these as incidental findings of no consequence unless they secrete hormones at levels sufficient to produce a named endocrine syndrome.

Within the coevolutionary framework described in this paper, the microadenoma cannot be simply classified as a neoplasm. It is a tissue stress response to sustained abnormal demand on the pituitary gland. This reinterpretation follows directly from the pituitary governance architecture described in Sections 4.3 and 5.7, and from the clinical progression documented in the longitudinal case study (Craddock, Hemodynamic Decompensation).

The archival clinical literature describes a specific mechanism: when the pituitary is driven into sustained overdrive by the organism's management program, the tissue responds with localized proliferation. This is not clonal expansion from a somatic mutation. It is a mechanical consequence of a gland operating beyond its design specifications. The resulting tissue

protrusion, termed a microgranuloma in the case study neurologist's assessment, is the visible signature of governance load.

4.7.1 Case Study: Pituitary Load Across Transition Phases

The longitudinal case study documents four transition events in which pituitary load is directly implicated:

Initial Transition to Phase 1 (1995). The subject presented with the first documented SIADH episode and electrolyte crisis, initiating polyuria that would persist for decades. Within this framework, this event marks the activation of the organism's pituitary governance program. The pituitary was induced into overdrive, distorting ADH output and producing the electrolyte dysregulation that conventional medicine classified as idiopathic SIADH. During this period, the subject documented hyphal transit along venous pathways from the forearm, tracking through the axilla, along the clavicle, up the neck, past the ear, and terminating behind the orbit, a trajectory consistent with venous return toward the cavernous sinus surrounding the pituitary fossa. The organism's remote governance of the pituitary via perfusion management and ECS signaling had been disrupted by the gland's entry into overdrive. Direct local access was the compensatory response. A subsequent dedicated pituitary MRI with contrast, obtained at the subject's insistence, identified a microgranuloma on the pituitary. The neurologist's response was reassurance: "These are commonly found in autopsies of people who died from other conditions." Within the governance load model, the microgranuloma was not an incidental finding. It was the tissue stress signature of a gland that had just been placed under a workload it was not designed to sustain indefinitely, with organism presence now established locally at the relay station.

Phase 1 to Phase 2 (2008). The subject experienced a salt/potassium imbalance event with cardiac involvement and possible ureter collapse. While the primary clinical presentation involved electrolyte-driven vascular and renal effects rather than direct pituitary symptoms, the event is consistent with escalating organism metabolic demand on a system already operating under sustained governance load. The remaining functional adrenal was maximally compensating, and the pituitary's management burden increased correspondingly.

Phase 2 to Phase 3 (2012). The subject presented with sustained buzzing sensation in the head followed by acute loss of muscle tone, and urinary shutdown subsequent to a CT with iodine contrast and administration of heparin (a “standard hospital protocol”). These symptoms map to the archival literature's description of a pituitary reaching its compensatory limit after prolonged overdrive. The concurrent administration of heparin during this period introduces a pharmacological confound that complicates precise attribution of symptoms to the pituitary transition versus anticoagulant effects. Nevertheless, the symptom cluster is consistent with the transition described in the source material as the point at which the gland recognizes it can no longer sustain its current output.

Phase 3 to Phase 4 (2018). The subject, already in a state of chronic volumetric depletion, donated blood. The organism's compensatory demand on the pituitary escalated over approximately 48 hours as the distributed system attempted to manage the additional volume deficit through increased ADH, ACTH, and related output (Craddock, Hemodynamic Decompensation). The microgranuloma, which had been identified on the earlier dedicated pituitary MRI with contrast and subsequently confirmed absent on later imaging, detached under this sustained mechanical load.

The clinical presentation resembled a pituitary apoplexy: acute onset, hormonal disruption, and transient neurological effects. However, the subject remained conscious throughout, was upright within two to three minutes, and was functional at blood pressures that conventional physiology would predict to be incompatible with ambulation. This resilience is consistent with a system that had spent twenty-three years developing compensatory architecture under organism governance, not with an incidental tumor producing a random vascular event.

Hyphal Migration and Direct Pituitary Access

The pituitary gland sits outside the blood-brain barrier. The hypothalamus and pituitary stalk lack the tight endothelial junctions that exclude blood-borne molecules and organisms from brain tissue. This anatomical accessibility is well established and is the basis for the perfusion governance model described in Section 4.3.

C. albicans hyphae possess documented capabilities relevant to directed tissue transit. Hyphae exhibit thigmotropism, sensing substrate topography and making tropic movements in relation to changes in surface contour (Sherwood *et al.*, 1992). They traverse host cells through trans-cellular tunnels that are progressively remodeled, in some cases without breaching host cell membranes (Lachat *et al.*, 2022). Active penetration is driven by turgor pressure at the hyphal tip and does not require host cellular machinery. The electrostatic surface charge of *C. albicans* is pH-dependent (Jones and O'Shea, 1994), meaning that changes in host acid-base status alter the physical interaction dynamics between hyphae and host tissue.

The hyphal transit documented during the 1995 initial transition (described above) provides the case study evidence for this directed access capability. The acute change in host acid-base chemistry as the pituitary entered overdrive altered the electrostatic interaction environment, and the organism's response was physical migration to the governance site via venous pathways terminating at the cavernous sinus. Once established at the pituitary, the organism possesses the molecular tools for a mode of management not accounted for in the two-tier endocrine interaction model described in Section 5.4.

The host side of this partnership is also prepared. Breuel *et al.* (2004) demonstrated that anterior pituitary somatomammotroph cells (rodent) and folliculostellate cells (human) express a glucan-specific binding site with sub-micromolar affinity (Kd 3.6–3.9 μM), and that coincubation with fungal glucan increases prolactin accumulation by 56–62% over media-alone controls and upregulates TLR4 and CD14 gene expression. The pituitary does not merely receive fungal signals incidentally; it carries dedicated pattern recognition machinery for fungal cell wall components and produces a measurable hormonal output in response. This is a host-side interface architecture for fungal-pituitary communication that does not require hyphal arrival — circulating glucan, present in patients with fungal infections (Breuel *et al.*, 2004), engages pituitary PRRs directly. The result is a two-channel architecture: hyphae present at the pituitary execute local hormone multiplexing through their own machinery (described below), while peripheral fungal load broadcasts a glucan-mediated activation signal that the pituitary is built to receive. Both channels converge on a single gland under organism governance. [The pituitary is architected to receive fungal signals. The receptors were already there. Selection ran on both sides of this conversation. It has been going on since the dawn of mammals.]

External clinical confirmation of the direct-access mechanism comes from a culture-proven case of intrasellar *C. albicans* abscess in a 36-year-old HIV-negative woman with T-cell dysfunction (Heary, Maniker, & Wolansky, 1995). The presentation included menstrual irregularities and mild diabetes insipidus that preceded diagnosis by twelve months — a

posterior-pituitary failure pattern consistent with the early-onset signature this paper's framework predicts when the organism establishes presence at the gland. The authors performed an extensive workup to identify the systemic source of the candidal seeding: blood (arterial and venous), sputum, urine, cerebrospinal fluid, nasopharynx, oral mucosa, skin, vagina, and cervix were each cultured. All sites returned no growth or normal flora. The pituitary was the only location where pathological *C. albicans* was recovered. The case report defaulted to "presumed hematogenous spread from an unidentified source" because the standard model has no other interpretation available when the workup fails to find a systemic origin. [*The interstitium wasn't a recognized anatomical compartment until 2018. Everything the 1995 workup could sample came back clean. The framework is not constrained to a list of suspects from 1995.*]

Local Hormone Multiplexing: A Communication Layer Beyond Receptor Sensing

Section 5.4 documents the organism's eleven confirmed hormone-sensing channels and the two-tier endocrine interaction model in which the organism reads host hormones directly and writes pituitary output indirectly through perfusion and ECS governance. The presence of hyphae at the pituitary introduces a third tier: direct local hormone interception and modification.

C. albicans possesses documented molecular machinery for active hormone processing. The Cdr1p ABC transporter performs energy-dependent efflux of human steroid hormones, specifically beta-estradiol and corticosterone (Krishnamurthy *et al.*, 1998). The corticosteroid-binding protein (CBP) binds corticosterone with high affinity (Kd = 6.3 nM) without metabolizing it, effectively sequestering the hormone (Loose and Feldman, 1982). The estrogen-binding protein (Ebp1) is not a receptor homolog but an oxidoreductase, an enzyme that chemically modifies estradiol upon binding (Madani *et al.*, 1994). Additionally, *C. albicans* can convert androstenediol and androstenedione into testosterone *de novo* (cited in Soares *et al.*, 2019).

These are three distinct modes of hormone interaction: transport (Cdr1p efflux), sequestration (CBP binding), and enzymatic modification (Ebp1 oxidoreductase activity), plus *de novo* synthesis. An organism physically present at the pituitary with this toolkit can intercept, redirect, modify, and supplement hormone output at the source. This constitutes a multiplexed local management capability that operates independently of, and in addition to, the remote governance mechanisms described elsewhere in this paper.

This local multiplexing would be invisible to any conventional diagnostic modality. Imaging resolves the tissue stress response (the microadenoma) but cannot detect hyphae at the scale involved. Serum hormone assays measure net output after organism processing, not gross pituitary production. The gland may be under significant governance load while circulating hormone levels appear normal or borderline. The microadenoma is the only visible indicator that the pituitary is working harder than the bloodwork suggests.

Prevalence Epidemiology and the Governance Load Prediction

The epidemiological profile of pituitary microadenomas is consistent with the governance load interpretation and inconsistent with the conventional model of spontaneous benign neoplasia.

Prevalence ranges from 1.4% to 27% in autopsy studies depending on histological criteria and sectioning methods. Radiological prevalence is higher (up to 37% in some MRI series). The natural history of observed microadenomas shows 83% stable, 10% enlarging, and approximately 6% decreasing in size over follow-up periods of two to eight years. These are

cross-sectional snapshots. The critical observation is that microadenomas are rare in children, peak during reproductive years with female predominance, and show variable distribution in older populations.

This age and sex distribution is precisely what the governance load model predicts. The organism's endocrine management demands are highest during active reproductive cycling, when LH sensing, estrogen processing via Ebp1, progesterone-responsive CDR1 induction, and the full tier-one receptor suite are operating at maximum capacity. The pituitary is working harder because the organism is asking more of it. The tissue stress response (microadenoma) reflects this workload. The female predominance reflects the organism's documented responsiveness to reproductive hormones, not a sex-linked genetic predisposition to pituitary neoplasia.

A 30-year population-based analysis from Olmsted County, Minnesota (Graffeo *et al.*, 2022) documented a 4.5-fold increase in pituitary adenoma standardized incidence rates from 1989 to 2017, a trend observed independent of incidental diagnosis rates. Yuen *et al.* reported at least one anterior pituitary hormone abnormality in 50% of patients with nonsecreting microadenomas and normal IGF-1 levels. These are not nonfunctioning tumors. They are pituitaries under load, producing hormonal output that is being intercepted or is falling outside the narrow diagnostic windows of named endocrine syndromes.

Populations of Interest and the Missing Dataset

The governance load model generates a specific, testable prediction: microadenoma prevalence should correlate with colonization density. Populations with documented high *C. albicans* colonization burden should show elevated microadenoma rates compared to matched controls.

Chronic substance users represent a population of particular interest. Opioid use produces well-documented HPA axis suppression, with hypogonadism prevalence ranging from 21% to 86% of users and opioid-induced adrenal insufficiency now recognized as a clinical entity. The conventional interpretation attributes these endocrinopathies to direct opioid receptor effects at the hypothalamic-pituitary level. Within the governance load framework, exogenous opioids interact with a signaling channel the organism relies on (the endocannabinoid and opioidergic overlap), forcing compensatory pituitary overdrive. The pituitary is now under load from two directions: the drug's direct suppressive effects and the organism's compensatory escalation. This is an accelerated version of the governance load that produces microadenomas in the general population.

If a chronic user's microgranuloma detaches under this combined load, the resulting pituitary failure event produces acute hormonal dysregulation in a host without the compensatory architecture developed over decades in the longitudinal case study. The drive to self-medicate intensifies because the body has lost its endocrine governance. This is not addiction worsening. It is a pituitary structural failure being managed with the only pharmacological tool available to the patient.

No study has performed dedicated pituitary MRI with contrast on cohorts of chronic substance users compared to matched controls. No study has correlated quantitative Candida colonization assessment with microadenoma prevalence in any population. Such assessment must use detection methodology sensitive to the niche distribution and density variability the framework predicts; conventional fecal-sample-based mycobiome surveys understate true

colonization status by a substantial fraction (see §6 Counter-Argument 5; (Craddock, Pan-Mammalian)). These are the missing datasets.

Limitations and Open Questions

This section proposes the microadenoma as a tissue stress marker of organism governance load and identifies a previously unrecognized local hormone multiplexing capability. It does not claim to fully characterize the purpose of local pituitary management by the organism beyond the general principle documented throughout this paper: the organism modifies its host environment to optimize its own metabolic position.

The specific downstream consequences of local hormone interception, sequestration, and enzymatic modification at the pituitary source remain to be characterized. Whether the organism's local activity is primarily consumptive (using pituitary output as substrate), regulatory (modulating output to manage downstream host physiology), or both, cannot be determined from available data. The second-order effects of local hormone multiplexing on adrenal, thyroid, gonadal, and growth hormone axes are predictable in principle but unquantified.

The 2012 transition in the case study is confounded by concurrent heparin administration. The degree to which the observed symptoms reflect pituitary transition versus anticoagulant effects cannot be cleanly separated from available clinical records.

A further observational confound warrants explicit identification. The most commonly used CT contrast agent is iodine-based, and iodine has documented dose-dependent antifungal activity against C. albicans in both acute and chronic exposure windows (Cuellar-Rufino et al., 2022). Any CT-based investigation of pituitary organism presence simultaneously perturbs that presence at the imaging site, creating a methodological constraint: the imaging tool reduces the signal it would need to detect, in proportion to the local iodine dose. In the longitudinal case study, the 2013 CT with iodine contrast produced acute renal complications attributable to the iodine load relative to the subject's compromised filtration capacity. The framework predicts that the same iodine bolus would also have perturbed any organism presence in the pituitary region at the time of imaging, though this prediction is not directly demonstrable from the case-study data alone. Dedicated pituitary MRI with gadolinium contrast avoids the antifungal confound but does not resolve individual hyphae. The prediction described in this section may ultimately require novel imaging or histological approaches that do not destroy the target organism during observation.

What can be stated is that *C. albicans* possesses documented physical access to the pituitary (Section 4.3), documented molecular tools for hormone binding, transport, modification, and synthesis, and that the epidemiological profile of pituitary microadenomas is consistent with a governance load mechanism and inconsistent with a model of random benign neoplasia. The correlation studies that would test this interpretation have not been conducted.

IV.VIII Pharmacological Confirmation: The Antifungal Cascade as Measured Governance Disruption

Sections 4.3 and 4.7 describe organism-mediated pituitary governance and reframe the microadenoma as the tissue stress signature of that governance load. Those arguments rest on anatomy, molecular toolkit, and epidemiological distribution. This subsection adds a different class of evidence: what happens when you pharmacologically interfere with the organism's enzymatic infrastructure. If the governance model is correct, disrupting organism signaling nodes

should produce measurable, mechanism-consistent endocrine cascades in the host. Mainstream pharmacovigilance data confirm that this is precisely what occurs. The field has documented and quantified the cascade; it has not yet recognized what the cascade implies.

The Field's Own Admission

Thakkar *et al.* (2026), in a January 2026 narrative review in World Journal of Clinical Cases, catalog the endocrine consequences of antifungal therapy under the explicit title "A Missed Entity." The review documents azole-induced adrenal insufficiency across multiple mechanistic pathways, apparent mineralocorticoid excess from posaconazole and itraconazole, reproductive dysfunction with ketoconazole, voriconazole-induced hyponatremia via SIADH or salt-losing nephropathy, fluoride-related periostitis from voriconazole and itraconazole, hypoglycemia from voriconazole and ketoconazole, and nephrogenic diabetes insipidus from amphotericin B via aquaporin-2 suppression. Every endocrine axis this paper identifies as subject to organism governance appears in Thakkar's catalog of antifungal adverse effects. The authors attribute these effects to cytochrome P450 interference and direct tubular toxicity, mechanisms that account for individual enzyme interactions but not for the breadth of the systemic endocrine signature produced by drugs targeting a specific fungal sterol synthesis enzyme. [*This is the "unexplained but documented" position mainstream endocrinology now occupies. The mechanism they need is the one this paper provides: the drug is hitting governance infrastructure, not just a pathogen.*]

The Pharmacovigilance Signal

Ji *et al.* (2022), in Antimicrobial Agents and Chemotherapy, performed a disproportionality analysis of the FDA Adverse Event Reporting System database through 2020 Q4 for triazole-associated apparent mineralocorticoid excess (AME). Their findings establish the quantitative weight of the cascade:

- Posaconazole: reporting odds ratio 865.37 (95% CI 464.14–1613.45)
- Itraconazole: reporting odds ratio 556.21 (95% CI 303.05–1020.85)
- Fluconazole, voriconazole, isavuconazole: no significant signal

A supplementary systematic review identified 66 clinical AME cases following posaconazole or itraconazole exposure (mean age 55.5 years; range 6–87), with median time to event onset of 11.5 weeks and a serum concentration threshold above 3 μg/mL for posaconazole-associated events (mean 4.4 μg/mL; events rare below 2 μg/mL).

Reporting odds ratios in this range are extreme. Most pharmacovigilance signals producing regulatory label changes land below 50. An ROR of 865 with a tight lower confidence bound indicates an effect the database has measured with high reliability against the full comparator of every other drug in the system.

The Mechanistic Split Is Diagnostic

The clean separation between azoles that produce the AME signal and those that do not is not a pharmacokinetic artifact. Posaconazole and itraconazole inhibit 11β-hydroxysteroid dehydrogenase type 2 (11β-HSD2) and/or 11β-hydroxylase (CYP11B1); these are the drugs that produce AME. Fluconazole, voriconazole, and isavuconazole do not inhibit these enzymes; these are the drugs that produce no signal. The signal tracks the mechanism with precision.

The implication is that the AME cascade is not a general toxicity phenomenon but the consequence of disrupting a specific mineralocorticoid-regulation node. Within this paper's framework, that node is part of organism-host governance infrastructure. The organism runs mineralocorticoid balance in part through enzymatic control at 11β-HSD2 and 11β-hydroxylase; pharmacological inhibition of those enzymes reveals the pathway by breaking it.

A Dose-Response Across Drug Classes

The prediction that falls out of this framing is testable against existing data. If antifungals produce endocrine cascades proportional to how specifically they disrupt organism enzymatic infrastructure, then drugs that hit more central governance nodes should produce broader cascades, and drugs that hit targets absent from organism-host governance should produce minimal cascades.

Amphotericin B, which binds the shared sterol backbone (ergosterol in the organism; cholesterol analogs in the host), hits the most central possible target. Thakkar documents the broadest cascade for this drug: nephrogenic diabetes insipidus via aquaporin-2 suppression, renal tubular acidosis, potassium and magnesium wasting, secondary hypoparathyroidism via hypomagnesemia-induced PTH dysfunction, and hypocalcemia. The cascade spans the full axis this paper identifies as under organism management.

Echinocandins (caspofungin, micafungin, anidulafungin) inhibit β-1,3-glucan synthase, an enzyme with no mammalian analog and no role in the governance architecture described in Sections 4.3 and 5.4. Thakkar reports that this class "rarely affects endocrine pathways," with isolated reports of hypercalcemia and dose-dependent hypokalemia of unclear mechanism.

The antifungal pipeline offers a forward-looking test of the same logic. Several agents in current clinical development target fungal-specific enzymes outside the sterol and glucan pathways, achieve central nervous system exposure sufficient to reach the pituitary governance site, are fungistatic rather than fungicidal against *Candida*, and do not inhibit their mammalian orthologs. Drugs with this combined profile would be predicted by the framework to produce a measurably different endocrine adverse event signature than either the fungicidal azoles (which collapse governance through cell death plus enzymatic disruption of 11β-HSD2, CYP11B1, and CYP17A1) or amphotericin B (which hits the shared sterol backbone). The expected profile is gradual attenuation of governance-related endocrine signaling as the organism loses its tissue foothold, rather than the acute cascades documented by Ji *et al.* and Thakkar *et al.* An agent that strips organism anchoring at governance sites without breaking host enzymes is the cleanest available test of whether the cascades described in this subsection reflect pharmacological governance disruption or general drug toxicity. One example of a drug in this category currently advancing through clinical trials is fosmanogepix, a GPI-anchor biosynthesis inhibitor targeting the fungal Gwt1 enzyme.

[The dose-response across classes tracks the framework. Mainstream pharmacology has no explanation for why a glucan-synthesis inhibitor should be endocrine-sparing while a sterol inhibitor should produce systemic endocrine collapse. The framework's answer: the glucan-synthesis target is not part of the governance system; the sterol target is.]

Implications for Populations on Chronic Antifungal Therapy

The 11.5-week median onset in Ji *et al.* places AME in chronic-dose territory. This is the duration profile where the framework predicts sustained pharmacological disruption of governance enzymes should overwhelm host compensation. The population that experiences this

cascade most reliably is, unsurprisingly, the population on the longest continuous antifungal regimens: patients with chronic mucocutaneous candidiasis requiring indefinite suppressive therapy. The APECED cohort is the most extensively documented example (Rautemaa *et al.*, 2007; Siikala *et al.*, 2010). Their multi-axis endocrine failure has historically been attributed entirely to their AIRE-mediated autoimmunity. The data reviewed in this subsection indicate that a meaningful fraction of their endocrine decompensation may reflect pharmacological governance disruption superimposed on autoimmune injury, a possibility that has not been investigated in existing longitudinal datasets.

The same logic applies to any chronically suppressed population: hematologic malignancy patients on posaconazole prophylaxis, solid organ transplant recipients on voriconazole, cystic fibrosis patients on itraconazole for allergic bronchopulmonary aspergillosis, HIV patients on maintenance fluconazole. Each of these cohorts shows endocrine manifestations in the literature; each has been studied in isolation without the unifying framework that organism governance disruption would provide.

IV.IX Systematic Diagnostic Blind Spots: Standard Panels Designed for a Different Patient

The preceding sections describe an organism that modulates electrolyte handling, renal function, and acid-base chemistry as core features of its governance program, and document the endocrine cascade that results when that program is pharmacologically disrupted (§4.8). Standard clinical laboratory panels are designed to detect acute pathology in patients with stable body composition and intact metabolic baselines. When the organism's long-term management program alters those baselines, the panels do not fail randomly. They fail systematically, and in each case the direction of the failure is the same: the result looks better than the underlying physiology warrants.

Urine bicarbonate was once a standard component of urinalysis and electrolyte panels. It is the single most informative measurement for evaluating renal tubular acidosis, a condition in which the kidney fails to appropriately acidify urine despite systemic acidosis. Within the framework, RTA is a predictable consequence of organism-mediated electrolyte manipulation at the renal tubule, where documented Na^+/K^+-ATPase interactions (Section 5.5e) and pH engineering capabilities (Section 4.2) converge on the same tissue. Urine bicarbonate was removed from standard panels. The stated rationale was cost efficiency and low diagnostic yield in the general population. The consequence is that the measurement most likely to detect organism-driven renal tubular dysfunction is no longer performed unless specifically ordered by a clinician who already suspects RTA, a condition whose diagnosis requires the very test that was removed. The longitudinal case study subject's 2012 laboratory panel illustrates the result: a comprehensive metabolic workup that included serum electrolytes but did not include the urine bicarbonate measurement that would have identified the renal tubular contribution to his documented chronic acidosis.

Creatinine-based estimated glomerular filtration rate presents a different failure mode with the same directional bias. The Cockcroft-Gault and MDRD equations calculate renal filtration capacity from serum creatinine concentration, using body weight and demographic variables as proxies for muscle mass. Creatinine is a metabolic byproduct of skeletal muscle turnover. The equations assume stable muscle mass because they were validated in populations with stable muscle mass. In any subject undergoing significant muscle catabolism, whether from

the organism's substrate progression through host tissue (documented in the longitudinal case study and in the archival clinical literature referenced in Section 4.7.1), from cancer cachexia, from prolonged immobility, or from anorexia nervosa (itself a stuck-state condition within this framework), creatinine production declines as the tissue generating it is consumed. Serum creatinine falls. The eGFR equation interprets falling creatinine as improved renal function. The test reads normal, or even elevated, precisely when actual filtration capacity may be declining. The bias is unidirectional: in any subject with progressive muscle loss, eGFR always overestimates kidney function. It never underestimates it. By the time serum creatinine rises enough to flag abnormal function, the subject has lost sufficient muscle mass that the denominator of the equation has collapsed. The result is a patient whose renal function appeared stable on every panel drawn during the years when intervention might have changed the trajectory.

These blind spots have direct consequences for the antifungal cascade documented in the preceding section. If antifungal administration disrupts organism governance infrastructure and produces the endocrine failures cataloged by Thakkar *et al.* (2026) and quantified by Ji *et al.* (2022), then detecting those failures early requires measurements sensitive to the specific axes being disrupted. The governance model predicts that organism-mediated electrolyte management would be among the first systems to destabilize under antifungal pressure, producing measurable shifts in urinary sodium, potassium, bicarbonate, and osmolality before serum values move far enough to trigger conventional flags. Urinary salt profiling before, during, and after antifungal courses would provide the earliest and most sensitive window into governance disruption, at negligible cost, using technology that has existed for over a century. No antifungal monitoring protocol currently includes these measurements. The most informative early signal of the cascade documented in §4.8 is not being collected in any clinical setting.

The pattern across all three examples is structural, not incidental. The diagnostic infrastructure was optimized for a population whose baseline physiology does not include an organism managing electrolyte balance, acid-base chemistry, and substrate mobilization as part of a long-term governance program. The panels were not designed to detect this patient. The antifungal monitoring protocols were not designed to measure what the drug is actually disrupting. In each case, the missing measurement is the one that would make the organism visible.

5. Testable Predictions

The biochemical computer model frames *C. albicans* as a distributed processing system: it senses inputs via dedicated sensors/transporters, computes responses through parallel pathways, and deploys context-specific outputs via morphology- and vesicle-dependent mechanisms. Its orphan genes, codon reassignment, parasexual cycle, and multi-layered interfaces supply the hardware. The predictions below test these components at molecular, cellular, and population scales. They are ordered by increasing technical demand to reflect a realistic feasibility hierarchy. Positive results would strengthen the integrated architecture; null or opposing results would falsify or require refinement of specific sub-models.

5.1 Genetic and Reproductive Foundations

Prediction 1: Orphan gene functional signatures.

Analysis of the ~1,300 *C. albicans*-specific genes using genomic foundation models (e.g., *Evo 2* or successors) will reveal enriched signatures consistent with host-interaction roles, including predicted GPCR ligands, neuropeptide-mimicking sequences, or regulatory elements for peptide processing. Method: chromosome-by-chromosome variant-effect scoring, sparse autoencoder feature extraction, and clustering against known symbiont or mammalian prohormone substrates. Enrichment for interaction motifs would support expanded hardware for the control surface; absence would weaken claims of deep co-evolutionary integration.

Prediction 2: Parasexual recombination as regulated bet-hedging.

Under host-mimicking stresses (low oxygen, glucose depletion, sub-inhibitory antifungals), parasexual progeny will display greater phenotypic variance in virulence traits (hyphal elongation, biofilm matrix, EV cargo diversity) and improved survival in macrophage/epithelial assays compared with mitotic clones. Method: mating-type homozygosis, tetraploid formation, ploidy reduction, single-cell phenotyping, and whole-genome sequencing. Stress-dependent diversity gains (absent under benign conditions) would confirm parasex as a controlled subroutine; lack of elevation would falsify its bet-hedging role.

Prediction 2a: Genome-wide heterozygosity partitioning by function.

Across the 182-isolate *C. albicans* population dataset (Ropars *et al.*, 2018) and the SC5314 phased diploid reference (Muzzey *et al.*, 2013), genes annotated for environmental sensing, metabolite calibration, and reference-point reporting will show enrichment for LOH homozygosity relative to the genome-wide baseline, while genes annotated for secreted effectors, adhesion, efflux, and phenotypic-switch regulation will show enrichment for retained heterozygosity. Method: intersection of *Candida* Genome Database gene coordinates with published heterozygous-block and LOH-block boundary calls, stratified by Gene Ontology category and by curated functional lists. Significant enrichment in the predicted directions would validate the committed-input / parallel-output architecture as a genome-wide feature; absence of enrichment would indicate that the pattern observed at the well-characterized loci examined in Section 2.2 is due to study-selection bias rather than architectural design.

Prediction 2b: Bimodal ancestry of orphan genes.

Application of genomic foundation models (e.g., Evo 2) to the ~1,300 *C. albicans*-specific genes (Butler *et al.*, 2009) under the hybrid-origin framework (Mixão and Gabaldón, 2020) will reveal a bimodal distribution of ancestral origin, with subsets aligning with one or the other inferred parental lineage rather than a unimodal distribution indicating single-lineage origin. Method: haplotype phasing of orphan gene sequences, clustering against reconstructed parental haplotype profiles, and comparison against null distributions from non-orphan genes with known orthologs. A bimodal signature would support the hybrid-origin attribution of the expanded host-interaction gene families; a unimodal signature would indicate that orphan genes are post-hybridization innovations rather than inherited parental contributions.

5.2 Signaling Inputs

Prediction 3: Hgt4 as high-affinity glucose sensor calibrated to host physiology.

Wild-type *C. albicans* will exhibit an inflection in HGT4-dependent transcriptional responses (induction of HGT12, HXT10, HGT7) and morphological outputs (yeast-to-hyphal transition) near 5 mM extracellular glucose (human serum range), while a constitutively signaling Hgt4 variant drives hyper-filamentation even at lower levels, and an hgt4Δ mutant shows defective growth and hypofilamentation on low-glucose media. Method: dose-response curves (0.1–10 mM glucose) with qRT-PCR/reporter assays and filamentation scoring. Precise calibration to ~5 mM with corresponding virulence phenotypes would validate Hgt4 as a tuned input sensor for host glucose homeostasis; lack of inflection would refute host-specific sensory adaptation. The *in vitro* form of this prediction has not been completed, and its *in vivo* mammalian extension — Hgt4-mediated transcriptional response tracking host blood glucose excursions in colonized animal models on dietary substrate manipulation, with paired host endpoint measurement — remains entirely uninvestigated. The gap is itself diagnostic of the field's investigational priorities: the calibration of a fungal sensor to human serum glucose has been characterized in defined media but not against the host parameter the calibration is tuned to. Closing this gap is a Clear Evidence candidate.

Prediction 4: Peptide transporters as dual nutrient/sensor channels.

Exposure of wild-type *C. albicans* (versus the septuple OPT/PTR transporter mutant) to physiologically relevant host gut-derived peptide hormones (GLP-1, CCK, PYY) or neuropeptides (Substance P, NPY) will elicit measurable transcriptomic or morphological responses (e.g., altered hyphal induction, pH alkalinization genes, or SAP expression). Because these peptides exceed the typical substrate size for direct OPT/PTR transport (2–8 amino acids), the response is predicted to depend on prior extracellular proteolytic processing by secreted aspartyl proteases (SAPs) to generate importable fragments. Method: RNA-seq or fluorescent reporter assays after exposure in defined media, with parallel assays in SAP-deficient mutants to confirm the two-step (proteolysis → import) requirement. Attenuated responses in the transporter mutant (or in SAP-deficient strains) would demonstrate that these transporters function as environmental sensors in addition to their nutritional role; no difference would restrict them to purely nutritional functions.

Prediction 5: Cholinergic interface bidirectionality (long-term validation target)

Acetylcholine or muscarinic agonists will inhibit biofilm formation and hyphal transition *in vitro* (reversed by scopolamine). Reciprocally, colonized versus germ-free murine gut models are predicted to differ in host acetylcholine levels and vagal tone metrics, scaling with fungal burden. Method: *in vitro* biofilm assays for direct fungal response; ex vivo/*in vivo* choline/acetylcholinesterase and vagal signaling measurements for host-side effects. This reciprocal test is technically demanding and best suited as longer-term validation. Clear bidirectional modulation would confirm a functional cholinergic channel; absence of host-side changes would falsify interface status.

5.3 Processing and Output Layers

Prediction 6: EV-mediated cross-kingdom sRNA transfer and gene silencing.

Purified hyphal EVs incubated with human epithelial cells or macrophages will deliver detectable fungal-origin sRNAs that produce AGO-dependent downregulation of predicted immune or metabolic target transcripts. Method: small RNA-seq of recipient cells ± host AGO knockdown or ESCRT-mutant EVs. Functional silencing would support EVs as a coordinated RNA output channel; no transfer/silencing would refute this layer.

Prediction 7: Codon optimization in EV-associated mRNAs.

EV-associated mRNAs will exhibit codon usage shifted toward human optimality (relative to bulk transcriptome), consistent with evasion of host DHX29 surveillance. Method: codon bias analysis of EV cargo versus whole-cell RNA. Human-optimized profiles would indicate co-evolutionary tuning; lack of shift would weaken refined RNA output claims. (Separable from sRNA silencing; one can succeed while the other fails.)

Prediction 8: Arachidonic acid competition linking prostaglandin mimicry to ECS tone.

In colonized mucosal/ex vivo gut models with biofilm (vs. uncolonized controls and ole2/fet3 mutants), PGE_2 will rise while host endocannabinoids (AEA, 2-AG) fall, scaling with fungal burden. Method: targeted lipidomics under controlled arachidonic acid supplementation. Reciprocal shift attenuated in mutants would confirm substrate competition as a core processing node; no crosstalk would undermine the shared lipid economy. External empirical confirmation of both downstream arms of this prediction — eCB-mediated HPA dysregulation rescued by FAAH inhibition, and PGE_2-mediated behavioral effects reversed by receptor antagonism — has been consolidated separately and is not recapitulated here (Craddock, AA Branch Point).

Prediction 8a: Adipokine and lipoprotein modulation as measurable colonization-density readouts.

Prospective human cohort stratification by quantitative mycobiome profiling will reveal colonization-density-dependent effects on fasting plasma leptin (inverse correlation), leptin/ghrelin ratio (shifted toward hunger), LDL-C, total cholesterol, and apolipoprotein B particle count (positive correlation), independent of BMI and dietary confounders. Method: deep metagenomic sequencing paired with standard lipid panel, leptin ELISA, and ghrelin ELISA across a density-stratified cohort ($n \geq 200$), with multivariate regression controlling for age, sex, BMI, fasting status, and gut bacterial composition. A secondary arm in familial hypercholesterolemia patients initiating ApoB-lowering therapy (mipomersen, lomitapide, or next-generation agents such as the DL-1 class) will track mycobiome composition before, during, and six months after treatment initiation; detection of a significant shift in *C. albicans* burden arbitrates the substrate-versus-defense balance, because reducing circulating ApoB simultaneously starves the organism of lipid substrate and removes the ApoB-derived antifungal cryptide patrol (Dell-Olmo, et al, 2021). A net decrease in fungal burden would indicate substrate limitation dominates; a net increase would indicate defense loss dominates. Dose-response correlation across both arms would validate host metabolic state as an output channel of the distributed biochemical computer; absence of correlation would weaken this claim and return LDL-C and leptin modulation to the status of coincidental colonization effects.

Prediction 9: EV-mediated CNS modulation via nasal-mucosal colonization route.

Madhu *et al.* (2026; Journal of Extracellular Vesicles) demonstrated that intranasally administered human neural stem cell-derived extracellular vesicles cross the blood-brain barrier, are internalized by microglia, alter microglial gene expression toward an anti-inflammatory

phenotype, restore mitochondrial function, reduce amyloid-β plaque burden, and produce measurable cognitive improvement in animal models of neurodegeneration. This establishes the nasal-to-CNS EV delivery route as anatomically patent and functionally consequential. The same route is continuously traversed by extracellular vesicles released from *C. albicans* colonizing the nasopharyngeal and oral cavities — a chronic, endogenous analogue of the experimental Madhu intervention. The biochemical computer model predicts that this delivery channel is not incidental but is a documented output vector of the distributed system, with inverse valence relative to the therapeutic reference.

Specifically:

(a) Biodistribution prediction. Fluorescently labeled *C. albicans* biofilm-derived EVs introduced into the nasal cavity of mice will show detectable accumulation in brain parenchyma, with preferential localization to microglia, on a timescale and at a magnitude comparable to the intranasal mammalian EV reference (Madhu *et al.*, 2026). Method: lipophilic dye-labeled hyphal EVs (distinguished from yeast EVs per Martínez-López *et al.*, 2022) administered intranasally, with brain sections imaged at 2, 6, 24, and 72 hours; co-localization with Iba1+ microglia quantified; mammalian EV positive control run in parallel. Detection at comparable levels would confirm the route is functional for fungal EV cargo; absence would indicate that fungal EV biophysics (size, surface composition, stability) preclude this delivery channel despite the route's established patency.

(b) Functional consequence prediction. Chronic nasal colonization with *C. albicans* in mouse models will produce a microglial transcriptional signature in the inverse direction of the Madhu therapeutic effect: upregulation of proinflammatory markers, altered amyloid-β clearance capacity, and measurable changes in cognitive and behavioral assays over months of colonization. Method: standardized nasal inoculation protocol in C57BL/6 mice versus germ-free controls, with microglial RNA-seq, cytokine profiling, and cognitive testing (Morris water maze, novel object recognition) at 4, 12, and 26 weeks. An inverse transcriptional signature combined with measurable behavioral effects would demonstrate that chronic fungal EV delivery is functionally consequential at the CNS level and place *C. albicans* colonization in the upstream causal position for a class of neuroinflammatory states currently treated as idiopathic; absence would refute the CNS-output arm of the biochemical computer model and restrict fungal EV action to peripheral tissue effects.

The paired prediction, if confirmed, would establish that the organism's EV output system is not confined to local epithelial and immune modulation at the colonization site but extends, through documented anatomical routes established in the mammalian EV therapeutics literature, to direct modulation of central nervous system immune tone. This is the computational architecture's most consequential output channel if correct.

5.4 Spatial Multiplexing and Population-Level Computation

Prediction 10: Niche-specific parallel subroutines.

Spatial or single-cell transcriptomics/proteomics in stratified host-mimicking models will reveal concurrent micro-niche-specific programs: glucose harvesting/Hgt4 signaling in lumen yeast, amino acid-driven alkalinization + SAP activity in hyphae, lactate/ketone utilization inside macrophages. Heterogeneity will track local gradients rather than pure stochastic noise. Method: laser-capture or droplet-based single-cell omics. Spatial partitioning would validate distributed multiplexing; uniform expression would falsify context-dependent computation.

Prediction 11: Colonization density scaling population-level outputs.

Quantitative mycobiome profiling stratified by *C. albicans* density will correlate higher burden with increased intra-population transcriptomic heterogeneity and stronger collective signaling outputs (e.g., aggregate PGE_2 or EV cargo effects on immune cells), independent of strain genetics. Method: deep metagenomics + sorted single-cell RNA-seq. Density-dependent amplification would support the population as the functional "computer"; no correlation would indicate purely cell-autonomous behavior.

Prediction 12: Volatile organic compound (VOC) profiling as real-time output channel.

In colonized versus germ-free murine gut models or simulated gastric environments, a collagen/peptide-rich meal (mimicking bone broth) will trigger a measurable spike in *Candida*-derived organosulfur VOCs (onion-like dimethyl sulfide, dimethyl disulfide, etc.) detectable by headspace GC-MS, scaling with fungal burden and attenuated in SAP-deficient or kynurenine-pathway mutants. Method: real-time VOC sampling during postprandial window + parallel lipidomics for PGE_2/ECS tone. Positive correlation with postprandial warmth/anhidrosis markers would confirm volatiles as a morphology-dependent broadcast layer of the biochemical computer; absence would falsify the expanded output model.

Prediction 13: Host intervention as subroutine terminator.

Quantitative single-cell RNA-seq or live imaging of *C. albicans* populations in stratified gut models will show that an acute glucose bolus (mimicking your honey/pizza rescue) rapidly down-regulates hyphal-invasion and SAP-expression programs while restoring luminal yeast glucose-harvesting transcripts — but only in wild-type strains with intact Hgt4 and peptide-transporter machinery. Method: time-resolved transcriptomics pre- and post-bolus. Successful termination (return to commensal heterogeneity) would validate the population-level "computer" responds to host-level carbohydrate overrides; failure in mutants would falsify the feedback loop. Carbon-source state operating as a master regulatory input is supported by external work showing that glucose depletion alone produces approximately 50-fold sensitization of pheromone signaling and bypasses the white-opaque epigenetic switch normally required for sexual mating, with the authors explicitly positioning glucose-state-driven mating as the more ancestral program and the white-opaque switch as a recent *C. albicans*–specific elaboration (Guan, Tao, Li, *et al.*, 2023). Glucose state is therefore a state-level input controlling multiple coordinated programs, not a single-program trigger — strengthening the prediction that an acute glucose bolus reaches multiple program nodes simultaneously rather than acting through one isolated pathway. Independent review-level evidence catalogs the downstream phenotypic consequences of carbon-source state: glucose drives hyphal morphology, fast growth, rough cell wall, and thin biofilm; lactate drives yeast morphology, smooth cell wall, rather thick biofilm, and strong cytotoxicity; sucrose drives smooth cell wall and thick biofilm; galactose drives hyphal morphology with slow growth (Wu *et al.*, 2026, synthesizing Lok *et al.*, 2021; Alves *et al.*, 2017; Pemmaraju *et al.*, 2016; Ene *et al.*, 2012a, 2013; Jin *et al.*, 2004). The lactate phenotype is particularly diagnostic: lactate is the immune-cell glycolytic burst byproduct, and the organism's response to encountering it is to retain commensal-looking yeast morphology while increasing cytotoxicity — a state-input/coordinated-output signature consistent with the biochemical computer architecture rather than a single-output morphological response.

Collectively, these predictions provide direct, falsifiable tests of the input sensors (Hgt4, peptide transporters, cholinergic receptor), parallel processing pathways (prostaglandin/ECS

competition, EV cargo), adaptive outputs (morphology, immune modulation), reproductive bet-hedging (parasex), and spatial multiplexing that together constitute the proposed biochemical computer. A coherent pattern of confirmatory results across layers would offer convergent empirical support; systematic failures at any layer would necessitate targeted revision. This roadmap prioritizes accessible molecular/cellular assays while identifying higher-complexity *in vivo* validations, ensuring the framework remains rigorously testable.

Prediction 14: Azole endocrine signatures track enzymatic governance targets.

In populations receiving chronic azole antifungal therapy, the breadth and timing of endocrine axis involvement will correlate with the drug's inhibitory profile against 11β-HSD2, 11β-hydroxylase, and CYP17A1, independent of the drug's inhibition of CYP3A4-mediated host drug interactions. Patients switched between azoles with different enzymatic profiles (e.g., posaconazole to isavuconazole) will show predictable rebalancing of endocrine manifestations consistent with the organism's resumed governance at nodes the prior drug was blocking. Patients maintained on echinocandins will show no comparable endocrine cascade despite equivalent organism suppression.

Prediction 15: Chronic apoB suppression alters mycobiome composition.

Patients on long-term high-intensity statin or PCSK9 inhibitor therapy will show measurable shifts in fecal and mucosal mycobiome composition, with *Candida* colonization burden inversely correlated with circulating apoB-cryptide-containing lipoprotein concentration. The effect will be amplified in patients with concurrent hepcidin axis compromise (chronic liver disease, anemia of chronic disease). Method: longitudinal mycobiome sampling stratified by lipid-lowering therapy and hepcidin status. Positive correlation would support apoB cryptides as a clinically active antifungal layer; absence of correlation would falsify the host-counter-measure reading.

Prediction 16: (formication mechanical and pharmacological response distinguishes biological from psychiatric mechanism)

In patients reporting formication during *Candida albicans* colonization, withdrawal, or post-antifungal die-off events, two bedside tests will distinguish biological from psychiatric mechanism. (a) Applied focal pressure at the reported sensation location will produce signature mechanical response — directional progression halts, local sensation persists at the pressure point — rather than the unchanged or randomly drifting sensation expected from centrally generated perceptual phenomenon. (b) Topical antifungal application to skin overlying the reported transit zone will reduce sensation within twenty-four hours on asymptomatic skin, consistent with direct organism interaction rather than central pharmacological mechanism. Method: structured bedside observation under blinded pressure-versus-no-pressure conditions and active-versus-vehicle topical conditions, in populations reporting formication during *Candida*-active states (post-antifungal die-off, methamphetamine use, polypharmacy with autonomic dysregulation). Positive results would establish formication-during-fungal-states as mechanically and pharmacologically responsive at the organism interface and inconsistent with hallucinatory mechanism. Negative results would falsify the hyphal-transit interpretation and return the symptom to the perceptual category.

6. Discussion & Conclusion

Candida albicans satisfies the four operational criteria of a biochemical computer: it senses inputs (Hgt4, peptide transporters, cholinergic receptor), integrates multiple signals (pH + temperature + nutrients → hyphal decision; biofilm feed-forward reinforcement), produces adaptive outputs (morphology, immune modulation via LILR engagement and candidalysin-mediated EGFR/CCNH hijacking, pH engineering), and maintains state across time through epigenetic phenotypic locking (white-opaque switching stabilized by Sir2/Hda1 complexes). Quorum sensing (farnesol/tyrosol), biofilm community organization, and host-signal crosstalk further support distributed, population-level computation.

The organism does not think, possess intentions, or exhibit consciousness. It carries a statistical record of past success encoded in its codon bias and regulatory architecture. Because the DNA sequence itself changes slowly, the population retains a bias toward reactions that proved successful in previous generations. Bet-hedging and parasexual recombination then act as the mechanism by which those historically successful states are re-tested and refined under new stress. In this sense the organism carries a form of long-term memory—not conscious recall, but a dynamic process of compiling numerous real-time inputs and cross-referencing them against its differential survival history. The more successful the response in the past, the more likely the architecture is to produce it again when similar conditions reappear. This is the essence of the biochemical computer: a distributed, chemical system that "remembers" what worked across deep evolutionary time without ever needing to think.

When the internal niche destabilizes, the same toolkit that supports commensalism shifts toward survival-oriented programs. This is not simple opportunism; it is reactive computation to changing host conditions.

Counter-Arguments and Limitations

Several reasonable objections can be anticipated. Critics may argue that the paper over-interprets existing data by assembling well-known individual capabilities into a "biochemical computer" narrative. Every individual finding cited is drawn directly from the peer-reviewed literature; what is novel is their synthesis into a unified functional description of a distributed, multi-channel processing system.

A second objection is that much of the evidence is *in vitro*. This is acknowledged, but the point cuts both ways. Where *in vivo* studies have been performed, they consistently verify that the proposed mechanisms occur inside living systems. At the same time, these experiments underscore the immense complexity of the real microbiome—with its hundreds of simultaneous inputs, micro-niches, oxygen gradients, pH fluctuations, and inter-species interactions that no single study can fully replicate. Far from weakening the model, this complexity lends it greater credibility: the more intricate the environment, the more adaptive and reactive *C. albicans* must be to persist.

Third, the description of *Candida albicans* as a biochemical computer may strike some readers as overly metaphorical. The model is strictly mechanistic: it describes distributed chemical computation via parallel channels and historical bias encoded in codon usage and regulatory architecture—nothing more. The organism does not think, does not possess intentions, and does not exhibit consciousness.

Fourth, the claim that no other known commensal matches this full toolkit will inevitably be challenged. To date, no other organism is known to combine bidirectional pH engineering, authentic host-mimetic prostaglandin production from host arachidonic acid, peptide-processing

machinery homologous to mammalian prohormone convertases, a functional cholinergic interface, EV-mediated RNA potential, and stress-gated parasexual diversity generation. Should future research identify such an organism, this uniqueness claim would of course require revision.

Fifth, a reader may object that conventional mycobiome surveys frequently report C. albicans absent in 30 to 60 percent of healthy humans, raising the question of whether the universal partnership architecture this paper describes is actually universal. The defensible answer is that apparent absence in the surveying literature reflects detection methodology limits rather than true biological absence. The cleanest evidence for this comes from veterinary work: the Foster canine mycobiome study found Candida sequence prevalence in healthy dogs ranging from 0 percent to 63.1 percent, with a median of 5.2 percent (Foster et al., 2013), despite dogs being presumably more uniformly colonized than humans through shared food bowls, grooming, and family contact. C. albicans has no known environmental reservoir and is acquired vertically from mother to child during birth canal transit and breastfeeding plus horizontally through close contact (Kumamoto, 2011). For 30 to 60 percent of adults to be genuinely Candida-free would require that fraction to have escaped vaginal birth, breastfeeding, family contact, and intimate contact with carriers — a population that does not exist. Standard surveys also sample wrong locations (stool samples reflect a single moment in the gut lumen while the organism's documented niches include skin, oral and genital mucosa, deep gut mucosa rather than lumen, the interstitium, and tissue compartments such as the perisellar venous network) and yeast-form quiescent populations and tissue-embedded hyphal networks are systematically underdetected by methods optimized for active luminal yeasts. The methodological argument is developed at length in (Craddock, Pan-Mammalian). For the framework's purposes, conventional detection rates should be read as detection-method-dependent rather than reflecting true biological state, and the partnership architecture described in this paper should be understood as operating in essentially all human hosts at varying density and tissue distribution.

Real-time longitudinal observations from the author’s documented physiological case study (Craddock, Redacted Science) provide *in vivo* corroboration of the expanded architecture. A recent peptide-rich load triggered postprandial central warmth, anhidrosis, and a strong organosulfur volatile signature — exactly the predicted integration/processing → output subroutine — which was terminated by a targeted carbohydrate bolus before tissue-remodeling programs engaged. These data illustrate the distributed biochemical computer operating under known inputs and demonstrate the practical utility of the model for interpreting symbiont-host dynamics in the living human system.

These counter-arguments are raised not to deflect criticism but to make transparent where the current limits of the evidence lie. The goal is not persuasion by rhetoric, but the presentation of a coherent, testable model that can be rigorously challenged with data.

This paper supplies technical grounding for the biochemical computer framework. It stands alone while providing molecular and genetic detail. The experimental roadmap in Section 5 offers clear paths to confirmation or falsification. Understanding *C. albicans* as a distributed regulator opens avenues in microbiology, immunology, metabolism, and host–microbe ecology. The refined signaling, memory, and output layers presented here, validated in real time by the Redacted Science longitudinal dataset, supply the mechanistic foundation for the *Mammalia candidus* / Saline Oscillation co-evolutionary framework developed in the companion manuscript.

References

1. Acharya, N., *et al.* (2017). Endocannabinoid system acts as a regulator of immune homeostasis in the gut. Proceedings of the National Academy of Sciences, 114(19), 5005–5010. https://doi.org/10.1073/pnas.1612177114

2. Arekar T, Katikaneni D, Kasem S, Desai D, Acharya T, Cole A, Khodayari N, Vaulont S, Hube B, Nemeth E, Drakesmith A, Lionakis MS, Mehrad B, Scindia Y. 2025. Essential role of hepcidin in host resistance to disseminated candidiasis. Cell Rep 44(5):115649. https://doi.org/10.1016/j.celrep.2025.115649

3. Bartelli, T. F., Bruno, D. C. F., & Briones, M. R. S. (2018). Evidence for mitochondrial genome methylation in the yeast *Candida albicans*: A potential novel epigenetic mechanism affecting adaptation and pathogenicity? Frontiers in Genetics, 9, 166. https://doi.org/10.3389/fgene.2018.00166 (PMC5986885)

4. Benias, P.C., Wells, R.G., Sackey-Aboagye, B., *et al.* (2018). Structure and distribution of an unrecognized interstitium in human tissues. Scientific Reports, 8, 4947. https://doi.org/10.1038/s41598-018-23062-6

5. Bezerra, A.R., *et al.* (2021). The role of non-standard translation in *Candida albicans* biology and pathogenesis. FEMS Yeast Research, 21(4), foab032. https://doi.org/10.1093/femsyr/foab032

6. Brand A, Vacharaksa A, Bendel C, Norton J, Haynes P, Henry-Stanley M, Wells C, Ross K, Gow NA, Gale CA. 2008. An internal polarity landmark is important for externally induced hyphal behaviors in *Candida albicans*. Eukaryot Cell 7(4):712-720. https://doi.org/10.1128/EC.00453-07

7. Brand A, Shanks S, Duncan VM, Yang M, Mackenzie K, Gow NA. 2007. Hyphal orientation of *Candida albicans* is regulated by a calcium-dependent mechanism. Curr Biol 17(4):347-352. https://doi.org/10.1016/j.cub.2006.12.043

8. Cuellar-Rufino, S., *et al.* (2022). Iodine induces toxicity against *Candida albicans* and *Candida* glabrata through oxidative stress. Iranian Journal of Microbiology, 14(2), 260–267. https://doi.org/10.18502/ijm.v14i2.9195

9. Joshua M. Borin, Justin J. Lee, Adriana Lucia-Sanz, Krista R. Gerbino, Joshua S. Weitz, Justin R. Meyer. Rapid bacteria-phage coevolution drives the emergence of multiscale networks. Science, 2023; 382 (6671): 674 https://doi.org/10.1126/science.adi5536

10. Brahma P, Aggarwal R, Sanyal K. 2023. Biased eviction of variant histone H3 nucleosomes triggers biofilm growth in *Candida albicans*. mBio 14(5):e02063-23. https://doi.org/10.1128/mbio.02063-23

11. Breuel, K. F., Kougias, P., Rice, P. J., *et al.* (2004). Anterior pituitary cells express pattern recognition receptors for fungal glucans: implications for neuroendocrine immune involvement in response to fungal infections. Neuroimmunomodulation, 11(1), 1–9. https://doi.org/10.1159/000072963

12. Brown, V., Sexton, J.A., & Johnston, M. (2006). A glucose sensor in *Candida albicans*. Eukaryotic Cell, 5(10), 1726–1737. https://doi.org/10.1128/EC.00186-06

13. Butler, G., *et al.* (2009). Evolution of pathogenicity and sexual reproduction in eight *Candida* genomes. Nature, 459(7247), 657–662. https://doi.org/10.1038/nature08064

14. Castro, M., Ralston, N. V. C., Morgenthaler, T. I., Rohrbach, M. S., & Limper, A. H. (1994). *Candida albicans* stimulates arachidonic acid liberation from alveolar macrophages through alpha-mannan and beta-glucan cell wall components. Infection and Immunity, 62(8), 3138–3145. https://doi.org/10.1128/iai.62.8.3138-3145.1994 (PMC302938)

15. Chen RC, Lan CY. 2020. Human Antimicrobial Peptide Hepcidin 25-Induced Apoptosis in *Candida albicans*. Microorganisms 8(4):585. https://doi.org/10.3390/microorganisms8040585

16. Cheng, S. C., van de Veerdonk, F. L., Smeekens, S., Joosten, L. A. B., van der Meer, J. W. M., Kullberg, B. J., & Netea, M. G. (2010). *Candida albicans* dampens host defense by downregulating IL-17 production. The Journal of Immunology, 185(4), 2450–2457. https://doi.org/10.4049/jimmunol.1000756

17. Craddock, J. The Arachidonic Acid Branch Point: External Empirical Confirmation. Architect Report AM#022. Redacted Science Research Initiative. https://doi.org/10.5281/zenodo.19983864

18. Craddock, J. Case Report - Acute Hemodynamic Decompensation Following Routine Phlebotomy in a Patient with Chronic Volume Dysregulation: A Five-Week Longitudinal Provocation Sequence. Zenodo. https://doi.org/10.5281/zenodo.19462705 [Cited as: Craddock, Hemodynamic Decompensation.]

19. Craddock, J. Redacted Science: The Pan-Mammalian Coevolution Hypothesis. Redacted Science Research Initiative. https://doi.org/10.5281/zenodo.19643601 [Cited as: Craddock, Pan-Mammalian.]

20. Craddock, J. Redacted Science [Book]. Distributed via IPFS, Nostr, ResearchGate, redactedscience.org. CID: bafybeidq7u7xbs526xvml6s6pbwq43rh7k5bzdrgkwlovwhw5oq2vhdrja [Cited as: Craddock, Redacted Science.]

21. Craddock, J. (2022). Longitudinal log and summary, jimcraddock.com. [Cited as: Craddock, 2022 log.]

22. Cravener, M.V., *et al.* (2023). Reinforcement amid genetic diversity in the *Candida albicans* biofilm regulatory network. PLoS Pathogens, 19(2), e1011109. https://doi.org/10.1371/journal.ppat.1011109

23. Davis-Hanna A, Piispanen AE, Stateva LI, Hogan DA. 2008. Farnesol and dodecanol effects on the *Candida albicans* Ras1-cAMP signalling pathway and the regulation of morphogenesis. Mol Microbiol 67(1):47-62. https://doi.org/10.1111/j.1365-2958.2007.06013.x

24. Dell'Olmo, E., Gaglione, R., Cesaro, A., Cafaro, V., Teertstra, W. R., de Cock, H., Notomista, E., Haagsman, H. P., Veldhuizen, E. J. A., & Arciello, A. (2021). Host defence peptides identified in human apolipoprotein B as promising antifungal agents. Applied Microbiology and Biotechnology, 105(5), 1953-1964. https://doi.org/10.1007/s00253-021-11114-3

25. Dumeaux, V., Massahi, S., Bettauer, V., *et al.* (2023). *Candida albicans* exhibits heterogeneous and adaptive cytoprotective responses to antifungal compounds. eLife, 12, e81406. https://doi.org/10.7554/eLife.81406 (PMC10699808)

26. Dunkel, N., *et al.* (2013). Roles of different peptide transporters in nutrient acquisition in *Candida albicans*. Eukaryotic Cell, 12(4), 520–528. https://doi.org/10.1128/EC.00008-13

27. Erb-Downward, J.R., & Noverr, M.C. (2007). Characterization of prostaglandin E_2 production by *Candida albicans*. Infection and Immunity, 75(7), 3498–3505. https://doi.org/10.1128/IAI.00232-07

28. Foster, M. L., Dowd, S. E., Stephenson, C., Steiner, J. M., & Suchodolski, J. S. (2013). Characterization of the fungal microbiome (mycobiome) in fecal samples from dogs. Veterinary Medicine International, 2013, Article 658373. https://doi.org/10.1155/2013/658373

29. Garbe, E., Thielemann, N., Hohner, S., Kumar, A., Vylkova, S., Kurzai, O., & Martin, R. (2023). Functional analysis of the *Candida albicans* ECE1 promoter. Microbiology Spectrum, 11(2), e00253-23. https://doi.org/10.1128/spectrum.00253-23

30. Glazier *et al.* (2023). The *Candida albicans* reference strain SC5314 contains a rare, dominant allele of the transcription factor Rob1 that modulates filamentation, biofilm formation, and oral commensalism. mBio, 14(5), e01521-23. https://doi.org/10.1128/mbio.01521-23

31. Guan, G., Tao, L., Li, C., *et al.* (2023). Glucose depletion enables *Candida albicans* mating independently of the epigenetic white-opaque switch. Nature Communications, 14, 2067. https://doi.org/10.1038/s41467-023-37755-8

32. Gutierrez, M. W., van Tilburg Bernardes, E., Ren, E., Kalbfleisch, K. N., Day, M., Lameu, E. L., *et al.* (2025). Early-life gut mycobiome core species modulate metabolic health in mice. Nature Communications, 16, Article 1467. https://doi.org/10.1038/s41467-025-56743-8

33. Halder LD, Babych S, Palme DI, et al. Candida albicans Induces Cross-Kingdom miRNA Trafficking in Human Monocytes To Promote Fungal Growth. mBio. 2022;13(1):e03563-21. https://doi.org/10.1128/mbio.03563-21

34. Hall RA, De Sordi L, Maccallum DM, Topal H, Eaton R, Bloor JW, Robinson GK, Levin LR, Buck J, Wang Y, Gow NA, Steegborn C, Mühlschlegel FA. 2010. CO2 acts as a signalling molecule in populations of the fungal pathogen *Candida albicans*. PLoS Pathog 6(11):e1001193. https://doi.org/10.1371/journal.ppat.1001193

35. Harpf V, Rambach G, Würzner R, Lass-Flörl C, Speth C. Candida and Complement: New Aspects in an Old Battle. Frontiers in Immunology. 2020;11:1471. https://doi.org/10.3389/fimmu.2020.01471

36. Heary, R. F., Maniker, A. H., & Wolansky, L. J. (1995). *Candida*l pituitary abscess: case report. Neurosurgery, 36(5), 1009–1013. https://doi.org/10.1227/00006123-199505000-00018

37. Hirakawa, M.P., *et al.* (2015). Genetic and phenotypic intra-species variation in *Candida albicans*. Genome Research, 25(3), 413–425. https://doi.org/10.1101/gr.174623.114

38. Holmes *et al.* (2006). Heterozygosity and functional allelic variation in the *Candida albicans* efflux pump genes CDR1 and CDR2. Molecular Microbiology, 62(1), 170–186. https://doi.org/10.1111/j.1365-2958.2006.05357.x

39. Iracane E, Vega-Estévez S, Buscaino A. 2021. On and Off: Epigenetic Regulation of *C. albicans* Morphological Switches. Pathogens 10(11):1463. https://doi.org/10.3390/pathogens10111463

40. Ji, H. H., Tang, X. W., Zhang, N., Huo, B. N., Liu, Y., Song, L., & Jia, Y. T. (2022). Antifungal therapy with azoles induced the syndrome of acquired apparent mineralocorticoid excess: A literature and database analysis. Antimicrobial Agents and Chemotherapy, 66(1), e01668-21. https://doi.org/10.1128/AAC.01668-21

41. Kornitzer, D. (2019). Regulation of *Candida albicans* hyphal morphogenesis by endogenous signals. Journal of Fungi, 5(1), 21. https://doi.org/10.3390/jof5010021

42. Joshi, A., Brahmandam, S., *et al.* (2026). CTG clade-specific proteins of the RSC chromatin-remodeling complex regulate cell cycle progression of a critical priority fungal pathogen, *Candida albicans*. mSphere, e00084-26. https://doi.org/10.1128/msphere.00084-26

43. Lesiak-Markowicz I, Vogl G, Schwarzmüller T, Speth C, Lass-Flörl C, Dierich MP, Kuchler K, Würzner R. *Candida albicans* Hgt1p, a multifunctional evasion molecule: complement inhibitor, CR3 analogue, and human immunodeficiency virus-binding molecule. J Infect Dis. 2011;204(5):802–809. https://doi.org/10.1093/infdis/jir455

44. Lin, J., *et al.* (2024). Global fungal-host interactome mapping identifies host targets of candidalysin. Nature Communications, 15, 1757. https://doi.org/10.1038/s41467-024-46141-x

45. Lionakis, M. S., Samonis, G., & Kontoyiannis, D. P. (2008). Endocrine and metabolic manifestations of invasive fungal infections and systemic antifungal treatment. Mayo Clinic Proceedings, 83(9), 1046–1060. https://doi.org/10.4065/83.9.1046

46. Lockhart *et al.* (2002). In *Candida albicans*, white-opaque switchers are homozygous for mating type. Genetics, 162(2), 737–745. https://doi.org/10.1093/genetics/162.2.737

47. Lohse, M.B., *et al.* (2009). White-opaque switching in *Candida albicans*. Current Opinion in Microbiology, 12(6), 650–654. https://doi.org/10.1016/j.mib.2009.09.010

48. Lu Y, Su C, Wang A, Liu H. Hyphal development in *Candida albicans* requires two temporally linked changes in promoter chromatin for initiation and maintenance. PLoS Biol. 2011;9(7):e1001105. https://doi.org/10.1371/journal.pbio.1001105

49. Luo S, Hoffmann R, Skerka C, Zipfel PF. The pH-regulated antigen 1 of *Candida albicans* binds the human complement inhibitor C4b-binding protein and mediates fungal complement evasion. J Biol Chem. 2011;285(11):8487–8499. https://doi.org/10.1074/jbc.M109.087874

50. Lu Y, Su C, Liu H. *Candida albicans* hyphal initiation and elongation: two phases of removing Nrg1 inhibition. Trends Microbiol. 2014;22(12):707–714. https://doi.org/10.1016/j.tim.2014.09.001

51. Madhu, L.N., et al (2026). Intranasal human NSC-derived EVs therapy can restrain inflammatory microglial transcriptome, and NLRP3 and cGAS-STING signalling, in aged hippocampus. Journal of Extracellular Vesicles, 15(2), e70232. https://doi.org/10.1002/jev2.70232

52. Meri T, Blom AM, Hartmann A, Lenk D, Meri S, Zipfel PF. 2004. The hyphal and yeast forms of *Candida albicans* bind the complement regulator C4b-binding protein. Infect Immun 72(11):6633-6641. https://doi.org/10.1128/IAI.72.11.6633-6641.2004

53. Midkiff, J., Borochoff-Porte, N., White, D., & Johnson, D. I. (2011). Small molecule inhibitors of the *Candida albicans* budded-to-hyphal transition act through multiple signaling pathways. PLoS ONE, 6(9), e25395. https://doi.org/10.1371/journal.pone.0025395 (PMC3180447)

54. Mishra, P. K., Baum, M., & Carbon, J. (2011). DNA methylation regulates phenotype-dependent transcriptional activity in *Candida albicans*. Proceedings of the National Academy of Sciences, 108(29), 11965–11970. https://doi.org/10.1073/pnas.1109631108 (PMC3141964)

55. Mishra, A., Forche, A., & Anderson, M.Z. (2021). Parasexuality of *Candida* species. Frontiers in Cellular and Infection Microbiology, 11, 796929. https://doi.org/10.3389/fcimb.2021.796929

56. Mixão, V., & Gabaldón, T. (2020). Genomic evidence for a hybrid origin of the yeast opportunistic pathogen *Candida albicans*. BMC Biology, 18, 48. https://doi.org/10.1186/s12915-020-00776-6

57. Mixão, V., Saus, E., Boekhout, T., & Gabaldón, T. (2021). Extreme diversification driven by parallel events of massive loss of heterozygosity in the hybrid lineage of *Candida albicans*. Genetics, 217(2), iyaa004. https://doi.org/10.1093/genetics/iyaa004

58. Moyes, D.L., *et al.* (2016). *Candida*lysin is a fungal peptide toxin critical for mucosal infection. Nature, 532(7597), 64–68. https://doi.org/10.1038/nature17625

59. Mühlhausen, S., *et al.* (2016). A novel nuclear genetic code alteration in yeasts and the evolution of codon reassignment in eukaryotes. Genome Research, 26, 945–955. https://doi.org/10.1101/gr.200931.115

60. Muzzey *et al.* (2013). Assembly of a phased diploid *Candida albicans* genome facilitates allele-specific measurements and provides a simple model for repeat and indel structure. Genome Biology, 14(9), R97. https://doi.org/10.1186/gb-2013-14-9-r97

61. Nile CJ, *et al.* (2019). Repurposing Pilocarpine Hydrochloride for Treatment of *Candida albicans* Infections. mSphere, 4(1), e00689-18. https://doi.org/10.1128/mSphere.00689-18

62. Peroumal, D., Sahu, S.R., Kumari, P., Utkalaja, B.G., & Acharya, N. (2022). Commensal fungus *Candida albicans* maintains a long-term mutualistic relationship with the host to modulate gut microbiota and metabolism. Microbiology Spectrum, 10(3), e01345-22. https://doi.org/10.1128/spectrum.01345-22

63. Qasim, M.N., *et al.* (2021). The roles of chromatin accessibility in regulating the *Candida albicans* white-opaque phenotypic switch. Journal of Fungi, 7(1), 37. https://doi.org/10.3390/jof7010037

64. Rai LS, Singha R, Sanchez H, Chakraborty T, Chand B, Bachellier-Bassi S, Chowdhury S, d'Enfert C, Andes DR, Sanyal K. 2019. The *Candida albicans* biofilm gene circuit modulated at the chromatin level by a recent molecular histone innovation. PLoS Biol 17(8):e3000422. https://doi.org/10.1371/journal.pbio.3000422

65. Rautemaa, R., Richardson, M., Pfaller, M., Koukila-Kähkölä, P., Perheentupa, J., & Saxén, H. (2007). Decreased susceptibility of *Candida albicans* to azole antifungals: A complication of long-term treatment in autoimmune polyendocrinopathy-candidiasis-ectodermal dystrophy (APECED) patients. Journal of Antimicrobial Chemotherapy, 60(4), 889–892. https://doi.org/10.1093/jac/dkm299

66. Ropars, J., *et al.* (2018). Gene flow contributes to diversification of the major fungal pathogen *Candida albicans*. Nature Communications, 9, 2253. https://doi.org/10.1038/s41467-018-04787-4

67. Santos, M.A., *et al.* (1995). The CUG codon is decoded *in vivo* as serine and not leucine in *Candida albicans*. Nucleic Acids Research, 23(8), 1481–1486. https://doi.org/10.1093/nar/23.8.1481

68. Shaw, K. J., & Ibrahim, A. S. (2020). Fosmanogepix: A review of the first-in-class broad spectrum agent for the treatment of invasive fungal infections. Journal of Fungi, 6(4), 239. https://doi.org/10.3390/jof6040239

69. Schlicker, E., & Kathmann, M. (2001). Modulation of transmitter release via presynaptic cannabinoid receptors. Trends in Pharmacological Sciences, 22(11), 565–572. https://doi.org/10.1016/S0165-6147(00)01805-8

70. Shivarathri R, Tscherner M, Zwolanek F, Singh NK, Chauhan N, Kuchler K. 2019. The Fungal Histone Acetyl Transferase Gcn5 Controls Virulence of the Human Pathogen *Candida albicans* through Multiple Pathways. Sci Rep 9:9445. https://doi.org/10.1038/s41598-019-45817-5

71. Siikala, E., Rautemaa, R., Richardson, M., Saxen, H., Bowyer, P., & Sanglard, D. (2010). Persistent *Candida albicans* colonization and molecular mechanisms of azole resistance in autoimmune polyendocrinopathy-candidiasis-ectodermal dystrophy (APECED) patients. Journal of Antimicrobial Chemotherapy, 65(12), 2505–2513. https://doi.org/10.1093/jac/dkq354

72. Singha R, Aggarwal R, Sanyal K. 2023. Negative regulation of biofilm development by the CUG-Ser1 clade-specific histone H3 variant is dependent on the canonical histone chaperone CAF-1 complex in *Candida albicans*. Mol Microbiol 119(5):574-585. https://doi.org/10.1111/mmi.15050

73. Staib *et al.* (2000). Differential activation of a *Candida albicans* virulence gene family during infection. Proceedings of the National Academy of Sciences, 97(11), 6102–6107. https://doi.org/10.1073/pnas.110031497

74. Staib & Morschhäuser (2010). Loss of heterozygosity at an unlinked genomic locus is responsible for the phenotype of a *Candida albicans* sap4Δ sap5Δ sap6Δ mutant. Eukaryotic Cell, 10(1), 54–62. https://doi.org/10.1128/EC.00281-10

75. Thakkar, S., Kantroo, V., Nagendra, L., Dutta, D., Kamrul-Hasan, A. B. M., Kalra, S., & Bhattacharya, S. (2026). Endocrine consequences of antifungal therapy: A missed entity. World Journal of Clinical Cases, 14(2), 117140. https://doi.org/10.12998/wjcc.v14.i2.117140

76. Thangamani, S., Monasky, R., Lee, J. K., Antharam, V., HogenEsch, H., Hazbun, T. R., Jin, Y., Gu, H., & Guo, G. L. (2021). Bile Acid Regulates the Colonization and Dissemination of *Candida albicans* from the Gastrointestinal Tract by Controlling Host Defense System and Microbiota. Journal of Fungi, 7(12), 1030. https://doi.org/10.3390/jof7121030

77. Vylkova, S., Carman, A. J., Danhof, H. A., Collette, J. R., Zhou, H., & Lorenz, M. C. (2011). The fungal pathogen *Candida albicans* autoinduces hyphal morphogenesis by raising extracellular pH. mBio, 2(3), e00055-11. https://doi.org/10.1128/mBio.00055-11

78. Wang, X., Zhou, S., Hu, X., Ye, C., Nie, Q., Wang, K., Yan, S., Lin, J., Xu, F., Li, M., Wu, Q., Sun, L., Liu, B., Zhang, Y., Yun, C., Wang, X., Liu, H., Yin, W.-B., Zhao, D., Hang, J., ... Chen, Z. (2024). *Candida albicans* accelerates atherosclerosis by activating intestinal hypoxia-inducible factor 2α signaling. Cell Host & Microbe, 32(6), 1002–1017.e8. https://doi.org/10.1016/j.chom.2024.04.017

79. Wu, J., Jiang, Y., Wang, Y., *et al.* (2026). The pathogenicity and future treatment strategies of *Candida albicans*. Frontiers in Cellular and Infection Microbiology, 16, 1752304. https://doi.org/10.3389/fcimb.2026.1752304

80. Xu XL, Lee RT, Fang HM, Wang YM, Li R, Zou H, Zhu Y, Wang Y. 2008. Bacterial peptidoglycan triggers *Candida albicans* hyphal growth by directly activating the adenylyl cyclase Cyr1p. Cell Host Microbe 4(1):28-39. https://doi.org/10.1016/j.chom.2008.05.014

81. Zarnowski, R., *et al.* (2018). *Candida albicans* biofilm-induced vesicles confer drug resistance through matrix biogenesis. PLoS Biology, 16(10), e2006872. https://doi.org/10.1371/journal.pbio.2006872

82. Zelante, T., Iannitti, R. G., Cunha, C., De Luca, A., Giovannini, G., Pieraccini, G., Zecchi, R., D'Angelo, C., Massi-Benedetti, C., Fallarino, F., Carvalho, A., Puccetti, P., & Romani, L. (2013). Tryptophan catabolites from microbiota engage aryl hydrocarbon receptor and balance mucosal reactivity via interleukin-22. Immunity, 39(2), 372–385. https://doi.org/10.1016/j.immuni.2013.08.003

83. Zhao *et al.* (2003). Allelic variation in the contiguous loci encoding *Candida albicans* ALS5, ALS1 and ALS9. Microbiology, 149(Pt 10), 2947–2960. https://doi.org/10.1099/mic.0.26488-0

84. Zhou X, Song N, Li D, Li X, Liu W. 2021. Systematic Analysis of the Lysine Crotonylome and Multiple Posttranslational Modification Analysis (Acetylation, Succinylation, and Crotonylation) in *Candida albicans*. mSystems 6:e01316-20. https://doi.org/10.1128/mSystems.01316-20